

## ORIGINAL RESEARCH ARTICLE



## Ezh2 Shapes T Cell Plasticity to Drive Atherosclerosis

Cecilia Assunta Bonfiglio<sup>1</sup> MD\*; Michael Lacy, PhD\*; Vasiliki Triantafyllidou, MSc; Floriana Maria Farina<sup>1</sup> PhD; Aleksandar Janjic<sup>1</sup> PhD; Katrin Nitz<sup>1</sup> PhD; Yuting Wu, MSc; Venetia Bazioti, PhD; Irem Avcilar-Kücükgoze, PhD; Yonara Freire Soares Marques, PhD; Markus Joppich<sup>1</sup> PhD; Mahadia Kumkum<sup>1</sup> MSc; Katja Röb, MSc; Anuroop Venkateswaran Venkatasubramani<sup>1</sup> PhD; Axel Imhof, PhD; Wolfgang Enard, PhD; Lars Maegdefessel<sup>1</sup> MD, PhD; Menno de Winther<sup>1</sup> PhD; Christian Weber<sup>1</sup> MD; Donato Santovito<sup>1</sup> MD, PhD; Esther Lutgens<sup>1</sup> MD, PhD\*; Dorothee Atzler<sup>1</sup> PhD†

**BACKGROUND:** The activation and polarization of T cells play a crucial role in atherosclerosis and dictate athero-inflammation. The epigenetic enzyme EZH2 (enhancer of zeste homolog 2) mediates the H3K27me3 (trimethylation of histone H3 lysine 27) and is pivotal in controlling T cell responses.

**METHODS:** To detail the role of T cell EZH2 in atherosclerosis, we used human carotid endarterectomy specimens to reveal plaque expression and geography of EZH2. Atherosclerosis-prone *ApoE* (apolipoprotein E)-deficient mice with CD (cluster of differentiation) 4<sup>+</sup> or CD8<sup>+</sup> T cell-specific *Ezh2* deletion (*Ezh2*<sup>cd4</sup>-knockout [KO], *Ezh2*<sup>cd8</sup>-KO) were analyzed to unravel the role of T cell *Ezh2* in atherosclerosis and T cell-associated immune status.

**RESULTS:** *EZH2* expression is elevated in advanced human atherosclerotic plaques and primarily expressed in the T cell nucleus, suggesting the importance of canonical EZH2 function in atherosclerosis. *Ezh2*<sup>cd4</sup>-KO, but not *Ezh2*<sup>cd8</sup>-KO, mice showed reduced atherosclerosis with fewer advanced plaques, which contained less collagen and macrophages, indicating that *Ezh2* in CD4<sup>+</sup> T cells drives atherosclerosis. In-depth analysis of CD4<sup>+</sup> T cells of *Ezh2*<sup>cd4</sup>-KO mice revealed that absence of *Ezh2* results in a type 2 immune response with increased *Il-4* (interleukin 4) gene and protein expression in the aorta and lymphoid organs. In vitro, *Ezh2*-deficient T cells polarized macrophages toward an anti-inflammatory phenotype. Single-cell RNA-sequencing of splenic T cells revealed that *Ezh2* deficiency reduced naive, Ccl5<sup>+</sup> (C-C motif chemokine ligand 5) and regulatory T cell populations and increased the frequencies of memory T cells and invariant natural killer T (iNKT) cells. Flow cytometric analysis identified a shift toward Th2 (type 2 T helper) effector CD4<sup>+</sup> T cells in *Ezh2*<sup>cd4</sup>-KO mice and confirmed a profound increase in splenic iNKT cells with increased expression of *Plzf* (promyelocytic leukemia zinc finger), which is the characteristic marker of the iNKT2 subset. Likewise, *Zbtb16* (zinc finger and BTB domain containing 16), the *Plzf*-encoding gene transcripts were elevated in the aorta of *Ezh2*<sup>cd4</sup>-KO mice, suggesting an accumulation of iNKT2 cells in the plaque. H3K27me3-chromatin immunoprecipitation followed by quantitative polymerase chain reaction showed that T cell-*Ezh2* regulates the transcription of the *Il-4* and *Zbtb16* genes.

**CONCLUSIONS:** Our study uncovers the importance of T cell EZH2 in human and mouse atherosclerosis. Inhibition of *Ezh2* in CD4<sup>+</sup> T cells drives type 2 immune responses, resulting in an accumulation of iNKT2 and Th2 cells, memory T cells and anti-inflammatory macrophages that limit the progression of atherosclerosis.

**Key Words:** atherosclerosis ■ epigenomics ■ EZH2 ■ natural killer T cells ■ T-lymphocytes

## Editorial, see p 1409

Correspondence to: Dorothee Atzler, PhD, Institute for Cardiovascular Prevention (IPEK), Klinikum der Universität München, Ludwig-Maximilians-Universität München (LMU Munich), Pettenkoferstr. 9, 80336 Munich, Germany, Email dorothee.atzler@med.uni-muenchen.de; or Esther Lutgens, MD, PhD, Department of Cardiovascular Medicine and Immunology, Experimental Cardiovascular Immunology Laboratory, Mayo Clinic, 200 First St SW, Rochester, MN 55905, Email lutgens.esther@mayo.edu  
\*C.A. Bonfiglio and M. Lacy contributed equally.  
†E. Lutgens and D. Atzler contributed equally.

This manuscript was sent to Andrew H. Baker, Guest Editor, for review by expert referees, editorial decision, and final disposition.

Supplemental Material is available at <https://www.ahajournals.org/doi/suppl/10.1161/CIRCULATIONAHA.124.072384>.

For Sources of Funding and Disclosures, see page 1406.

© 2025 The Authors. *Circulation* is published on behalf of the American Heart Association, Inc., by Wolters Kluwer Health, Inc. This is an open access article under the terms of the [Creative Commons Attribution Non-Commercial-NoDerivs](https://creativecommons.org/licenses/by-nc-nd/4.0/) License, which permits use, distribution, and reproduction in any medium, provided that the original work is properly cited, the use is noncommercial, and no modifications or adaptations are made.

*Circulation* is available at [www.ahajournals.org/journal/circ](http://www.ahajournals.org/journal/circ)

## Clinical Perspective

### What Is New?

- The expression of the epigenetic writer EZH2 (enhancer of zeste homolog 2) is increased in advanced atherosclerotic plaques and is associated with an unstable phenotype.
- The main source of EZH2 in advanced human atherosclerotic plaques are T cells.
- Deficiency of Ezh2 in T cells reduces atherosclerosis by inducing a type 2 immune response, characterized by induction of Il-4 (interleukin 4).
- Deficiency of Ezh2 in T cells favors polarization of iNKT2 (invariant natural killer T) and type 2 T helper cells, resulting in polarization of anti-inflammatory macrophages, as well as protective innate CD (cluster of differentiation) 8<sup>+</sup> memory cells.

### What Are the Clinical Implications?

- Therapies targeting T cell EZH2 have the potential to induce a type 2 immune response, which may reduce plaque inflammation and increase plaque stability.

## Nonstandard Abbreviations and Acronyms

<b>Ccl</b>	C-C chemokine ligand
<b>Ccr</b>	C-C chemokine receptor
<b>CD</b>	cluster of differentiation
<b>Cxcr3</b>	C-X-C motif chemokine receptor 3
<b>EZH2</b>	enhancer of zeste homolog 2
<b>Foxp3</b>	forkhead box protein 3
<b>H3K27me3</b>	histone 3 lysine 27 trimethylation
<b>IFN-<math>\gamma</math></b>	interferon- $\gamma$
<b>iNKT</b>	invariant natural killer T cell
<b>KO</b>	knockout
<b>NK</b>	natural killer
<b>PLZF</b>	promyelocytic leukemia zinc finger
<b>qPCR</b>	quantitative polymerase chain reaction
<b>scRNA-seq</b>	single-cell RNA sequencing
<b>Th</b>	T helper cell (types 1 and 2)
<b>Treg</b>	T regulatory cell
<b>Zbtb16</b>	zinc finger and BTB domain containing 16

**A**therosclerosis is a chronic, lipid-driven inflammatory disorder of the middle- and large-sized arteries that drives cardiovascular disease, including myocardial infarction and stroke.<sup>1,2</sup> A myriad of experimental evidence, including single-cell RNA sequencing (scRNA-seq) and mass cytometry studies, has identified many immune cell subsets as key components in human

and mouse atherosclerotic lesions with T cells representing an abundance of the lesional leukocytes.<sup>3,4</sup> Among those, many T cell subsets including CD (cluster of differentiation) 4<sup>+</sup> T helper (Th) subsets, CD4<sup>+</sup> T regulatory cells (Treg), and CD8<sup>+</sup> cytotoxic T cell subsets, as well as double-negative CD4<sup>+</sup>CD8<sup>-</sup> cells and invariant natural killer T (iNKT) cells, have been identified in plaques.<sup>5</sup> In humans, CD4<sup>+</sup> and CD4<sup>+</sup>/CD8<sup>-</sup> T cells are expanded in plaques from symptomatic patients and display distinct activation and differentiation patterns compared with asymptomatic patients.<sup>6–9</sup> Unraveling specific pathways that regulate T cell activation and differentiation in the context of atherosclerosis will enhance our understanding of atherogenesis; targeting these cells and pathways has a great potential to identify novel immunotherapeutic targets.

T cell differentiation, polarization, and activation are tightly controlled by epigenetic enzymes, which can restrict the expression of lineage-specific transcription factors and cytokines in effector T cells and help maintain long-term immunologic responses that may influence the outcome of chronic inflammatory diseases.<sup>10,11</sup> In particular, the expression of fate-determining transcription factors can depend on epigenetic mechanisms controlling their histone methylation status.<sup>12</sup> Notably, repressive histone marks, such as H3K27me3 (trimethylation of lysine 27 on histone 3), are pivotal in silencing ectopic T helper-associated gene expression in opposing subsets.<sup>13</sup> Enzymes responsible for methylation and demethylation intricately maintain the appropriate methylation level of the repressive mark H3K27me3. The di- and trimethylation of the histone residues are mediated by the PRC2 (polycomb repressive complex 2), composed by the core protein EZH2 (enhancer of zeste homolog 2) or its paralog EZH1, SUZ12 (suppressor of zeste 12), and accessory protein JARID2 (Jumonji and [A+T]-rich interaction domain-containing protein 2).<sup>14–17</sup> The repressive activity of the PRC2 is counterbalanced by 2 demethylases, UTX ([ubiquitously transcribed tetratricopeptide repeat, X chromosome], KDM6a [lysine demethylase 6A], JmjC [Jumonji C] domain-containing proteins) and JMJD3 ([Jumonji domain-containing protein-3] KDM6b [lysine demethylase 6B]).<sup>18,19</sup> EZH2 plays a pivotal role in regulating multiple subtypes of immune cells by mediating their activation, proliferation, and differentiation.<sup>20</sup> EZH2 activates macrophages and their inflammatory responses.<sup>21,22</sup> In T cells, EZH2 is involved in the development and differentiation of various T cell subsets including CD4<sup>+</sup> Th, CD8<sup>+</sup> memory T cells, Tregs, iNKT, and T follicular helper cells.<sup>23–26</sup> Beyond its epigenetic functions, EZH2 may act in a noncanonical, chromatin-independent manner.<sup>27,28</sup>

Here, we found that *EZH2* expression is elevated in human atherosclerosis and is primarily located in the nucleus of T cells. T cell-specific *Ezh2* deficiency in mice resulted in a significant decrease in atherosclerotic

plaque burden. This was mediated via the propagation of a type 2 immune response, particularly by iNKT2 and Th2 cells.

## METHODS

The authors declare that all data that support the findings of this study are available within the article or [Supplemental Material](#). Sequencing data are publicly available at the Gene Expression Omnibus (accession codes GSE283002 and GSE283191). Expanded descriptions of methods and materials can be found in the online supplement, according to ARRIVE (Animal Research: Reporting of In Vivo Experiments) guidelines.

### Human Samples

Human carotid artery plaques were collected from patients who underwent carotid endarterectomy. Written informed consent was given by each patient. The study protocol was approved by the regional ethical committee. After surgery, the biopsies were frozen or transferred to RNAlater and processed in the Munich Vascular Biobank.<sup>29,30</sup> Paraffin-embedded sections were subjected to immunohistochemical staining, as well as RNA extraction and gene expression analysis ([Supplemental Material](#)).

### Analysis of Human scRNA-seq Data

We retrieved single-cell gene expression data from the data sets generated as part of Alsaigh et al<sup>31</sup> and Bashore et al,<sup>32</sup> available through the Gene Expression Omnibus (accession codes GSE159677 and GSE253904, respectively). The pipeline for data analysis and visualization is described in the [Supplemental Material](#).

### Murine Studies

*Ezh2*<sup>fl/fl</sup> mice containing LoxP (locus of crossover P1)-flanked exons 14 and 15 of the *Ezh2* gene were provided by Stuart H. Orkin, Boston Children's Hospital.<sup>33</sup> To establish CD4<sup>+</sup> and CD8<sup>+</sup> cell-specific KO mice, *Ezh2*<sup>fl/fl</sup> mice were bred with *Cd4*<sup>cre</sup> (No. 017336; Jackson Laboratory)<sup>34</sup> or *Cd8*<sup>cre</sup> mice (provided by Andreas Thiel, Charité Berlin).<sup>35</sup> These mice were backcrossed  $\geq 10$  times with *Apoe*<sup>-/-</sup> mice (No. 002052; Jackson Laboratory) and genetic background was confirmed by genome-wide single nucleotide polymorphism analysis (Charles River). To induce atherosclerosis, mice were fed a Western-type diet (21% fat, 0.2% cholesterol; Ssniff) for 6 to 8 weeks. Mice were bred and housed in environmentally enriched cages with a 12-hour light/12-hour dark cycle at the animal facility at Ludwig Maximilians Universität München, according to institutional guidelines. To minimize confounders, animals were kept in standard conditions at all times. The experiments were performed and analyzed in a blinded fashion at all stages. The mice included in the experiments were monitored once per week according to a scoring system for animal disease and pain, which was approved by the local authorities. All animal experiments were approved by the local ethical committee for animal experimentation (animal protocol number 55.2Vet-2532.Vet\_02-17-180 and 02-22-150). The total number of mice used is indicated in [Table S7](#).

## Statistical Analysis

Data are presented as mean $\pm$ SD, unless noted differently. For data sets with  $n > 6$ , Gaussian distribution was examined using the Shapiro-Wilk test. Comparisons between 2 groups were analyzed by Student *t* test or Mann-Whitney *U* test, when the assumption of normal distribution was violated. To reduce the risk of inflation of the  $\alpha$  error, multiple ( $> 3$ ) comparisons were corrected with the false discovery rate approach described by Benjamini, Krieger, and Yekutieli, with a cutoff of 5%. Categorical variables were compared using  $\chi^2$  test or Fisher exact test, using GraphPad Prism v.10 software (GraphPad Software Inc, USA) and IBM SPSS Statistics v.29.0.2 (IBM Corporation, USA). Individual data points were excluded if identified as outliers by the ROUT (robust regression and outlier removal) test ( $Q = 1\%$ ) or excluded for genotyping and technical issues (eg, damaged sections). A 2-sided *P* value  $< 0.05$  was considered statistically significant.

## RESULTS

### EZH2 Transcripts Are Elevated in Human Atherosclerosis and Primarily Expressed in T Cells

Analysis of RNA-sequencing data from human carotid atherosclerotic plaques of the Munich Vascular Biobank<sup>29</sup> revealed a 1.7-fold increase ( $P = 2.0 \times 10^{-7}$ ) in *EZH2* expression in advanced atherosclerotic plaques compared with early lesions (proximal adjacent tissue; Figure 1A). Additionally, quantitative polymerase chain reaction (qPCR) analysis revealed significantly higher *EZH2* expression in unstable versus stable atherosclerotic plaques, classified according to established clinical and histomorphological criteria<sup>30</sup> ([Figure S1A and S1B](#)). To determine the cellular source of EZH2 within the human atherosclerotic plaque, we analyzed publicly available single-cell gene expression data (GSE253904) of 73 833 cells from 18 patients who underwent carotid endarterectomy.<sup>32</sup> Using established markers, we could identify all major immune cell types, as well as endothelial and smooth muscle cell clusters ([Figure S1C](#)). As visualized in the uniform manifold approximation and projection (UMAP), *EZH2* was primarily expressed in a distinct T cell subcluster, characterized by co-expression of proliferative genes (*TOP2A* [topoisomerase II $\alpha$ ], *TYMS* [thymidylate synthetase], *MKI67* [marker of proliferation Ki-67], and *PCLAF* [PCNA clamp associated factor]), which we termed *EZH2*<sup>+</sup> T cells, whereas lower expression was observed in other clusters, including Tregs, natural killer (NK) cells, dendritic cells, and macrophages (Figure 1B through 1E; [Figure S1C](#)). The prominent expression of *EZH2* in T cells compared with other cell types was confirmed in an independent scRNA-seq data set of human atherosclerotic plaques (GSE159677),<sup>31</sup> validating our findings ([Figure S1D and S1E](#)). These results suggest that T cell-derived *EZH2* contributes to atherosclerosis development and progression, warranting further investigations into its mechanistic relevance.

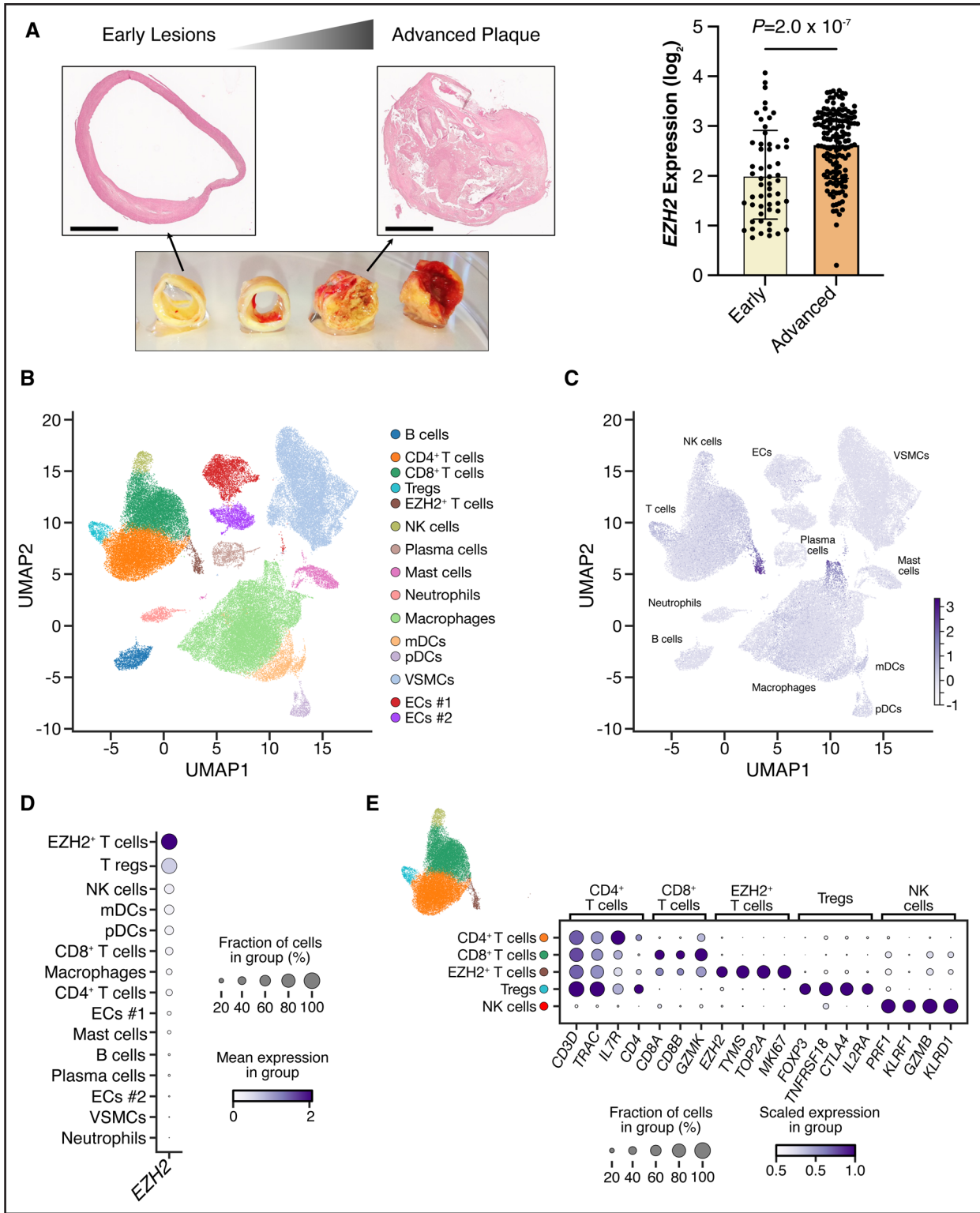


**Figure 1. *EZH2* expression is increased in human atherosclerotic carotid plaques and is predominantly present in plaque T cells.**

**A**, Representative images and hematoxylin and eosin staining (scale bar=2 mm) and *EZH2* (enhancer of zeste homolog 2) expression in advanced atherosclerotic plaques vs early lesions from bulk RNA-sequencing data of human carotid endarterectomy (CEA) samples of the Munich Vascular Biobank (n=56 vs 147). Data are presented as mean±SD and analyzed using a 2-tailed Mann-Whitney *U* test. **B** through **D**, Single-cell gene expression data were retrieved from a published data set of carotid atherosclerotic plaques from 18 patients who underwent CEA (GSE253904). **B**, Clusters of individual plaque T cells (CD4, CD8, Treg, and *EZH2*<sup>+</sup> cell subclusters), NK cells, B cells, plasma cells, dendritic cells (myeloid [mDCs] and plasmacytoid [pDCs]), neutrophils, mast cells, macrophages, endothelial cells (EC), and vascular smooth muscle cells (VSMC) visualized using the Uniform Manifold Approximation and Projection (UMAP). The cluster-defining genes are (Continued)

**Figure 1 Continued.** depicted in Figure S1C. **C**, Expression pattern of *EZH2* in individual cell clusters visualized in the UMAP. **D**, Dot plot depicting the relative expression of *EZH2* in each identified cell cluster from **C**. **E**, Zoom-in on the natural killer (NK) and T cell clusters in **B** with a dot plot showing the marker genes characterizing the 5 major subclusters. Color from white to purple in **C** through **E** represents average gene expression, whereas the dot size in **D** and **E** reflects the percentage of cells expressing the gene in each cluster. *CD3D* indicates CD3 delta subunit of T cell receptor complex; *CD4*, CD4 molecule; *CD8A*, CD8 subunit alpha; *CD8B*, CD8 subunit beta; *CTLA4*, cytotoxic T-lymphocyte associated protein 4; *EZH2*, enhancer of zeste homolog 2; *FOXP3*, forkhead box P3; *GZMB*, granzyme B; *GZMK*, granzyme K; *IL2RA*, interleukin 2 receptor subunit alpha; *IL7R*, interleukin 7 receptor; *KLRD1*, killer cell lectin like receptor D1; *KLRF1*, killer cell lectin like receptor F1; *MKI67*, marker of proliferation Ki-67; *PRF1*, perforin 1; *TNFRSF18*, TNF receptor superfamily member 18; *TOP2A*, topoisomerase II alpha; *TRAC*, T cell receptor alpha constant; and *TYMS*, thymidylate synthetase.

## Baseline Characteristics of T Cell-Specific *Ezh2*-Deficient Mice (*Ezh2*<sup>cd4-KO</sup>)

Because T cells are the major source of *EZH2* in human plaques, we studied T cell-specific *Ezh2* deficiency in atherosclerosis-prone *Apoe*<sup>-/-</sup> mice (*Ezh2*<sup>cd4-KO</sup>) and respective littermate controls (*Ezh2*<sup>cd4-WT</sup> [wild type]). Splenic T cells of atherosclerotic *Ezh2*<sup>cd4-KO</sup> mice showed a reduction of *Ezh2* at both the transcript (−72%) and protein (−90%) levels, as assessed by qPCR and immunofluorescence, confirming the specificity of the model (Figure S2A through S2C). Western blot and mass spectrometry-based analysis of histones isolated from CD4<sup>+</sup> T cells revealed a significant decrease in H3K27 di- and trimethylation in *Ezh2*<sup>cd4-KO</sup> mice (Figure S2C and S2D) compared with *Ezh2*<sup>cd4-WT</sup> littermates. Other components of the PRC2, such as *Ezh1*, *Suz12*, and *Jarid2*, as well as the demethylases *Utx* (*Kdm6a*) and *Jmjd3* (*Kdm6b*) remained unaffected in CD4<sup>+</sup> T cells (Figure S2A), suggesting no counter-regulation related to *Ezh2* deficiency. Body weight, basic hematological parameters, and plasma lipid profiles were comparable between *Ezh2*<sup>cd4-KO</sup> mice and littermates (Table S1).

## *Ezh2* Deficiency in T Cells Decreases Atherosclerosis

In the absence of T cell *Ezh2*, atherosclerotic plaque area was significantly decreased in aortic roots and arches of both female and male mice (Figure 2A; Figure S3A and S3B), compared with their *Ezh2*<sup>cd4-WT</sup> littermates. *Ezh2*<sup>cd4-KO</sup> mice had less advanced plaques (defined as fibrous cap atheroma) and a larger percentage of initial plaques (defined as intimal xanthoma and pathological intimal thickening),<sup>36</sup> suggesting that T cell *Ezh2* deficiency slowed plaque progression (Figure 2B). These findings were also reflected by changes in plaque composition: plaques of *Ezh2*<sup>cd4-KO</sup> mice had decreased collagen and macrophage content (Figure 2C and 2D) and no difference in  $\alpha$ -SMA<sup>+</sup> ( $\alpha$ -smooth muscle actin) cell content but a trend toward fewer CD4<sup>+</sup> T cells was observed (Figure 2E and 2F). The amount of lesional Foxp3<sup>+</sup> (forkhead box protein 3) Tregs was strongly reduced in *Ezh2*<sup>cd4-KO</sup> mice (Figure 2G). Collectively, these data indicate that *Ezh2* abrogation in T cells reduces atherosclerotic plaque size in both sexes, accompanied by altered plaque composition despite reduced Tregs.

## *Ezh2* Deficiency Profoundly Affects T Cell Populations

To further elucidate the effects of T cell *Ezh2* deficiency on the immune system, we analyzed the amount and composition of major immune cell (sub)populations in blood and lymphoid organs. *Ezh2* deficiency solely affected the number of CD3<sup>+</sup> T cells, whereas B cell, monocyte, and neutrophil counts remained unchanged in blood (Figure 3A). In-depth analysis of the T cell compartments in blood, lymph nodes, and spleen demonstrated that CD4<sup>+</sup> T cells were predominantly affected: *Ezh2*<sup>cd4-KO</sup> mice exhibited a decrease in CD4<sup>+</sup> T cells, whereas CD8<sup>+</sup> T cells were mainly unaltered (Figure 3B; Figure S3C). To further detail subpopulation differences in T cells, we employed scRNA-seq of splenic CD3<sup>+</sup> cells and identified 11 clusters of T cells (Figure 3C), characterized by using common expression markers (Figure S4A). *Ezh2*<sup>cd4-KO</sup> mice showed reduced percentages of naive CD4<sup>+</sup> and CD8<sup>+</sup> T cells, Ccl5<sup>+</sup> cells and Tregs, but increased percentages of CD4<sup>+</sup> and CD8<sup>+</sup> memory T cells, and especially iNKT cells (Figure 3D). These results were validated by flow cytometry: analysis of splenic CD4<sup>+</sup> T cells from *Ezh2*<sup>cd4-KO</sup> mice showed a shift from naive to effector memory T cells and a reduction in Tregs (Figure 3E; Figure S3D). Likewise, splenic CD8<sup>+</sup> T cells displayed a reduced naive fraction and a prominent central memory population (Figure 3D and 3F; Figure S3E). To better detail the profound increase in CD4<sup>+</sup> effector T cells, we analyzed subpopulations of effector memory cells using inflammatory chemokine markers, *Cxcr3* (C-X-C motif chemokine receptor 3) and *Ccr6* (C-C motif chemokine receptor 6), which are preferentially expressed on Th1 (type 1 T helper) and Th17 (type 17 T helper) cells, respectively.<sup>37–40</sup> Accordingly, we observed a shift from Th1 (*Cxcr3*<sup>+</sup>*Ccr6*<sup>+</sup>) to Th2 (*Cxcr3*<sup>+</sup>*Ccr6*<sup>−</sup>) cells in *Ezh2*<sup>cd4-KO</sup> mice (Figure 4A; Figures S3F and S7A). In line, we observed a trend toward elevated concentrations of the Th2-associated cytokines Il-4 and Il-13 in the plasma of *Ezh2*<sup>cd4-KO</sup> mice (Figure 4B). To confirm CD4<sup>+</sup> T cells as a cellular source of these cytokines, we stimulated CD4<sup>+</sup> T cells in vitro and subsequently measured cytokine release. The supernatant analysis demonstrated CD4<sup>+</sup> T cells from *Ezh2*<sup>cd4-KO</sup> mice secreted 39× more Il-4 and 8× more Il-13 compared with their *Ezh2*<sup>cd4-WT</sup> counterparts,

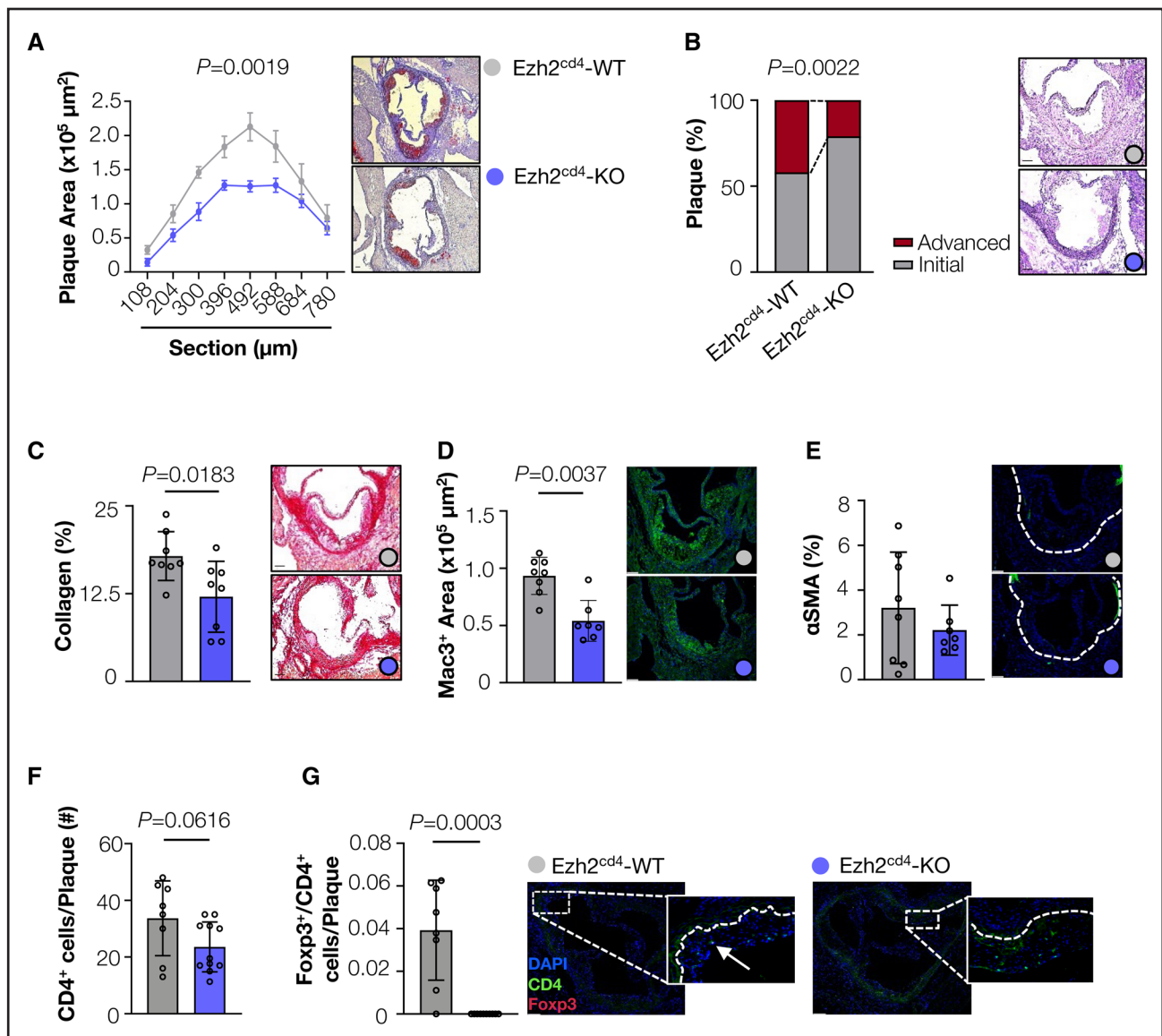


**Figure 2. T cell-specific *Ezh2* deficiency reduces plaque burden and determines fewer advanced plaques.**

**A**, Atherosclerotic plaque area at indicated positions across the aortic root in female *Ezh2*<sup>cd4</sup>-WT and *Ezh2*<sup>cd4</sup>-KO mice (n=8 vs 10) (left) with representative Oil Red O–stained images (right), scale bar: 100 μm. **B**, Atherosclerotic plaques classified by phenotype (initial and advanced plaques; n=24 lesions from 8 vs 8 animals) and representative hematoxylin and eosin–stained images (scale bar=100 μm). **C** through **E**, Histological and immunofluorescent quantification of collagen content through Sirius red analysis (**C**; n=8 vs 8), macrophage (Mac3<sup>+</sup>) area (**D**; n=8 vs 7), and αSMA (α-smooth muscle cell actin) content (**E**; n=8 vs 7) in cross-sections of the aortic root with representative images (scale bar=100 μm). **F** and **G**, Immunofluorescent staining assessing CD4<sup>+</sup> and Foxp3<sup>+</sup> cells in cross-sections of aortic roots with representative images (n=9 vs 10; scale bar=100 μm). Data are represented as mean±SD; comparisons were assessed by 2-tailed Student *t* test (**A**, **C**, and **F**), Fisher exact test (**B**), or 2-tailed Mann-Whitney *U* test (**D**, **E**, and **G**). For quantitative immunohistochemistry experiments, cohorts included 8 WT and 11 KO mice. Because of occasional section damage and folding, some samples had to be eliminated for some comparisons. *Ezh2* indicates enhancer of zeste homolog 2; Foxp3, forkhead box protein 3; KO, knockout; Mac3, macrophage surface protein, and WT, wild type.

with no change observed in the Th1-associated cytokine *Ifn-γ* ([interferon  $\gamma$ ] Figure 4C). Remarkably, we further observed a 17-fold increase of *Il-4* transcripts in the descending aorta of *Ezh2*<sup>cd4</sup>-KO mice, whereas *Ifn-γ* and *Il-13* remained unchanged (Figure 4D). These data suggest that deficiency of *Ezh2* in T cells favors the activation of systemic and local type 2 immune responses, possibly underlying the reduction in atherosclerosis.

### ***Ezh2* Deficiency in CD4<sup>+</sup> But Not CD8<sup>+</sup> T Cells Contributes to Type 2 Immune Responses in Atherosclerotic Mice**

To unveil the relevance of the changes in CD4<sup>+</sup> T and CD8<sup>+</sup> T cells for atherosclerosis upon T cell *Ezh2* deficiency, a second animal model with a CD8-specific *Ezh2* deficiency (*Ezh2*<sup>cd8</sup>-WT and *Ezh2*<sup>cd8</sup>-KO) was employed. CD8<sup>+</sup> T cells displayed a 60% reduction in *Ezh2* but

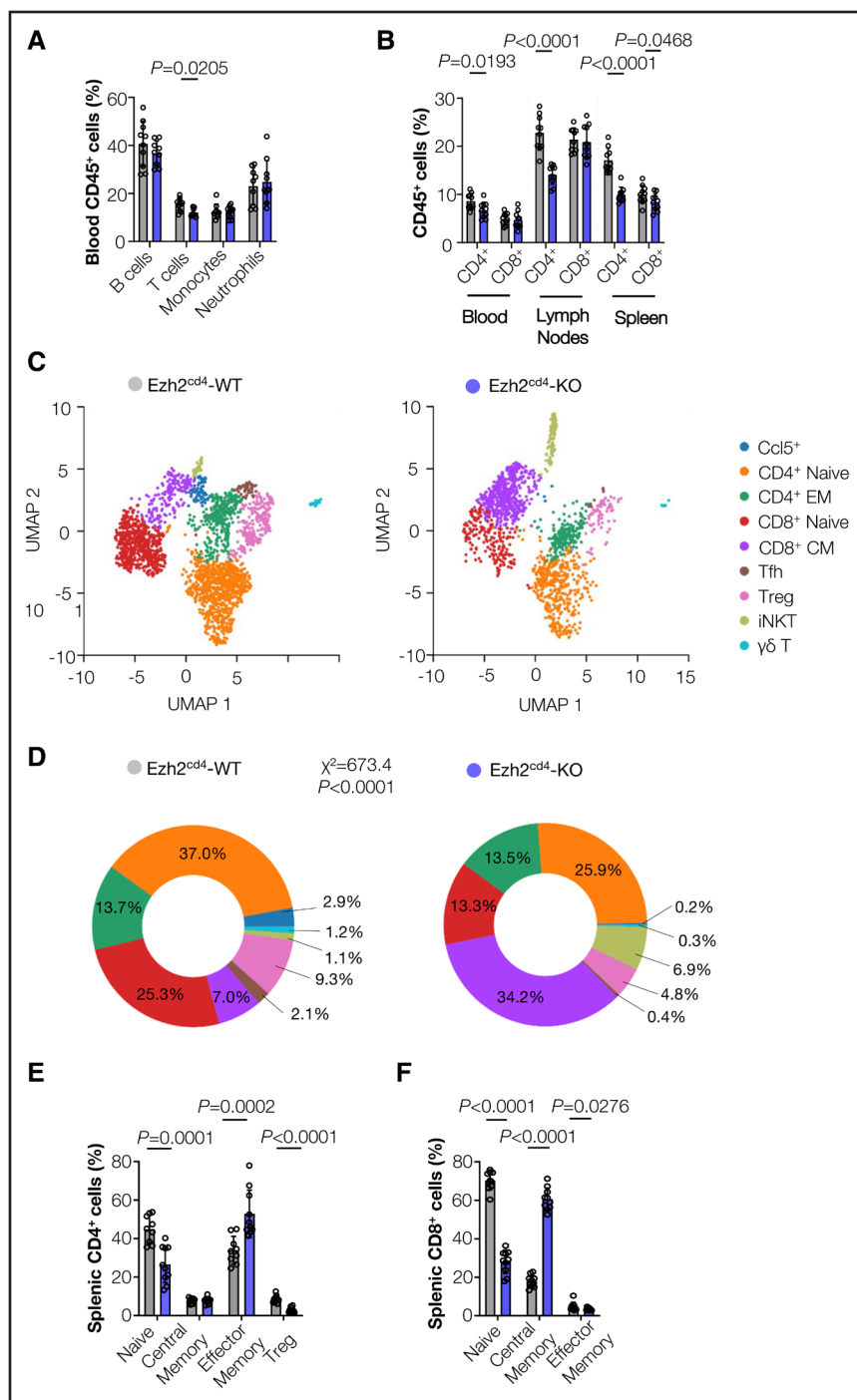


### Figure 3. T cell-specific *Ezh2* deficiency shifts T cell populations from naive to memory, effector and iNKT cell subsets.

**A**, Flow cytometric (FC) analysis of major blood immune cell populations in atherosclerotic *Ezh2<sup>cd4</sup>-WT* and *Ezh2<sup>cd4</sup>-KO* mice ( $n=9$  vs  $10$ ). **B**, FC analysis of the  $CD4^+$  and  $CD8^+$  subsets in the blood, lymph nodes (LN), and spleen ( $n=9$  vs  $10$ ). **C** and **D**, Single-cell transcriptomes of splenic  $CD3^+$  cells isolated from atherosclerotic *Ezh2<sup>cd4</sup>-WT* and *Ezh2<sup>cd4</sup>-KO* mice ( $n=4$  vs  $4$ ). **C**, Uniform Manifold Approximation and Projection (UMAP) visualization of cell clusters of individual  $CD3^+$  cell subsets in spleens from *Ezh2<sup>cd4</sup>-WT* and *Ezh2<sup>cd4</sup>-KO* mice. Cell clusters were annotated using cell-type specific marker genes, as depicted in Figure S4A. **D**, Doughnut chart visualizing the proportion of each T cell cluster identified using their single-cell transcriptome. **E** and **F**, FC analysis of splenic T cells isolated from *Ezh2<sup>cd4</sup>-WT* and *Ezh2<sup>cd4</sup>-KO* mice ( $n=9$  vs  $10$ ). **E**,  $CD4^+$  naive ( $CD62L^+$ ,  $CD44^-$ ), effector memory ( $CD62L^-$ ,  $CD44^+$ ), and Tregs, as well as  $CD8^+$ -naive, effector memory, and central memory T cells (**F**). Data are represented as mean  $\pm$  SD. **A**, **E**, and **F**, Comparisons were assessed using Mann-Whitney  $U$  tests with multiple comparisons and Benjamini-Krieger-Yekutieli correction for FDR, whereas in **B**, the analysis was performed per organ: multiple unpaired  $t$  tests for blood and multiple Mann-Whitney  $U$  tests for lymph nodes and spleen with multiple comparisons and Benjamini-Krieger-Yekutieli correction for FDR, for all the 3 organs. **D**, Comparisons were assessed with  $\chi^2$  test and post hoc Z tests corrected for Bonferroni. CD indicates cluster of differentiation; CD4em, CD4 effector memory; CD62L, CD62 antigen-like family member; CD8cm, CD8 central memory; *Ezh2*, enhancer of zeste homolog 2; *Foxp3*, forkhead box protein 3; iNKT, invariant natural killer T cells; KO, knockout; Tfh, T follicular helper cells; Treg, regulatory T cells; and WT, wild type.

not *Ezh1* transcripts (Figure S5A). Using Western blot analysis, we confirmed *Ezh2* deficiency in  $CD8^+$  T cells (Figure S5B). No significant differences were observed in basic hematological parameters or cholesterol levels of *Ezh2<sup>cd8</sup>-KO* mice and their WT littermates (Table S2). Plaque burden and development were unaltered in *Ezh2<sup>cd8</sup>-KO* mice fed a Western-type diet for 8 weeks compared to littermate controls (Figure S5C and S5D). Major immune cell populations in blood and lymphoid organs were unaffected by *Ezh2* deficiency in  $CD8^+$  T cells (Figure 5E). Moreover, proportions of  $CD4^+$  and  $CD8^+$  T

cells in blood, lymph nodes, and spleen were similar in *Ezh2<sup>cd8</sup>-KO* mice and littermate controls (Figure S5F). Considering the profound effects on T cell populations observed in *Ezh2<sup>cd4</sup>-KO* mice, we recapitulated the in-depth analysis of the T cell compartments. Splenic  $CD4^+$  T cells from *Ezh2<sup>cd8</sup>-KO* mice were mainly unaffected (Figure S5G), whereas splenic  $CD8^+$  T cells from *Ezh2<sup>cd8</sup>-KO* mice showed slight reductions in naive and effector memory subsets along with an increase in central memory T cells (Figure S5H). No differences were observed in Tregs (Figure S5G). Notably, plasma levels

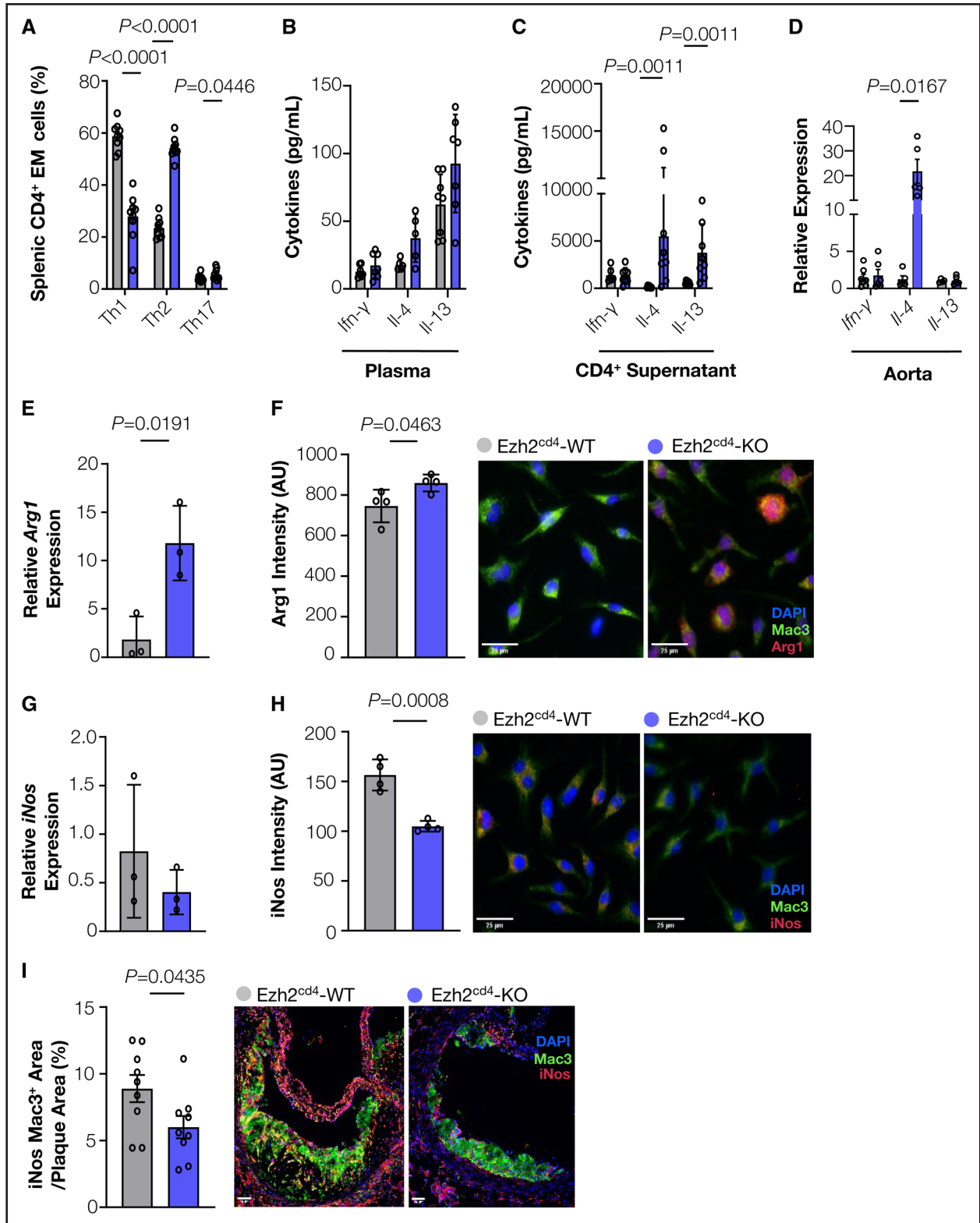


**Figure 4.** T cell-specific *Ezh2* deficient mice exhibit an increase in type 2 cytokine-producing T helper cells, capable of polarizing macrophages into an anti-inflammatory state.

**A**, Flow cytometric (FC) analysis of splenic CD4<sup>+</sup> T cells from atherosclerotic Ezh2<sup>cd4</sup>-WT and Ezh2<sup>cd4</sup>-KO mice to identify T helper (Th) 1 (Ccr3<sup>+</sup>/Ccr6<sup>-</sup>), Th2 (Ccr3<sup>-</sup>/Ccr6<sup>+</sup>) and Th17 (Ccr3<sup>+</sup>/Ccr6<sup>+</sup>) cells (n=9 vs 10). **B**, Cytokine measurements from the (B) plasma (n=5-8 vs 5-7) or (C) supernatant of in vitro cultured splenic CD4<sup>+</sup> T cells isolated from atherosclerotic Ezh2<sup>cd4</sup>-WT and Ezh2<sup>cd4</sup>-KO mice (n=7 vs 8). **D**, Gene expression of *Ifn-γ*, *Il-4*, and *Il-13* in the descending aorta of Ezh2<sup>cd4</sup>-WT and Ezh2<sup>cd4</sup>-KO mice (n=4-7 vs 5-6) using qPCR. **E** through **H**, Macrophage phenotyping after culturing with supernatant of CD4<sup>+</sup> T cells isolated from atherosclerotic Ezh2<sup>cd4</sup>-WT and (Continued)

**Figure 4 Continued.** Ezh2<sup>cd4</sup>-KO mice. **E**, Gene expression analysis of *Arg1* ([arginase 1] n=3 vs 3). **F**, Immunofluorescence *Arg1* (n=4 vs 4) with representative images (scale bar=25 μm). **G**, Gene expression analysis of inducible nitric oxide synthase ([iNos] n=3 vs 3). **H**, immunofluorescence staining of iNos (n=4 vs 4) with representative images (scale bar=25 μm). **I**, Immunofluorescent staining assessing macrophage (Mac3<sup>+</sup>) content and iNos-expressing macrophages in cross-sections of aortic roots with representative images (n=9 vs 9; scale bar=25 μm). Data are represented as mean±SD; comparisons were assessed with 2-tailed Student *t* test (**A**) and Mann-Whitney *U* tests (**B** through **D**) with multiple comparisons and Benjamini-Krieger-Yekutieli correction for false discovery rate, and with 2-tailed Student *t* test (**E** through **I**). CD indicates cluster of differentiation; Ezh2, enhancer of zeste homolog 2; KO, knockout; Mac3<sup>+</sup>, macrophage surface protein; and WT, wild type.

of type 2 cytokines (ie, Il-4 and Il-13) were unchanged in Ezh2<sup>cd8</sup>-KO mice (Figure S5I). Together, these data suggest that the CD8<sup>+</sup> T cell phenotype observed in our Ezh2<sup>cd4</sup>-KO model is not intrinsically related to *Ezh2* deficiency in CD8<sup>+</sup> T cells, but likely results from the effects of *Ezh2* deficiency in CD4<sup>+</sup> T cells. The type 2 immune response, and specifically the Il-4 environment induced by *Ezh2* deficiency in CD4<sup>+</sup> T cells, likely affects the phenotype and functionality of CD8<sup>+</sup> cells by skewing them toward (innate) memory traits.

### Ezh2 Deficiency in CD4<sup>+</sup> T Cells Polarize Macrophages Toward an Anti-Inflammatory State

Because T cells secrete cytokines with a profound effect on neighboring cells, we investigated whether T cells from Ezh2<sup>cd4</sup>-KO mice would regulate the polarization of surrounding macrophages. Indeed, when cultured with the supernatant from stimulated CD4<sup>+</sup> T cells from Ezh2<sup>cd4</sup>-KO mice, bone marrow-derived macrophages were polarized toward an anti-inflammatory phenotype, made evident via increased macrophage *Arg1* (arginase 1) mRNA and protein expression (Figure 4E and 4F). Additionally, inducible nitric oxide synthase (iNos), a key marker of inflammatory macrophages, was reduced after stimulation with Ezh2<sup>cd4</sup>-KO T cell supernatant (Figure 4G and 4H). In vivo, we found fewer iNos<sup>+</sup> macrophages in plaques of Ezh2<sup>cd4</sup>-KO mice (Figure 4I). These data together with the elevated aortic *Il-4* cytokine transcripts suggest that *Ezh2* deficient CD4<sup>+</sup> T cells may induce an advantageous, anti-inflammatory plaque macrophage phenotype, likely contributing to a reduction of atherosclerosis.

### Ezh2 Epigenetically Dampens the Differentiation of T cells Into iNKT Cells

To unravel mechanisms driving the identified effects on immune responses, we performed RNA sequencing on splenic CD4<sup>+</sup> T cells isolated from Ezh2<sup>cd4</sup>-KO mice and Ezh2<sup>cd4</sup>-WT controls using an efficient sequencing method (ie, Prime-seq).<sup>41</sup> Of 23 160 detected genes, we observed differential expression for 435 transcripts for a false discovery rate <5% (Figure 5A). Notably, the 187 upregulated genes in our transcriptomic analysis overlapped with those found to be regulated by H3K27me3 marks detected by chromatin-immunoprecipitation (ChIP) and sequencing in multiple cell types, including lymphoid subtypes (ENCODE [Encyclopedia of DNA Elements]

Histone Modification 2015; Figure 5B), thus corroborating that transcriptional changes are likely to reflect lower H3K27me3 repressive marks upon *Ezh2* deletion. Beyond confirming the increase in *Il-4* and other genes involved in type 2 immune response (Gene Ontology [GO]: 0042092;  $P=3.3\times 10^{-6}$ ), we identified an enrichment (factor >1.5) in pathways and processes relevant to lymphocyte differentiation and lymphocyte-mediated immunity. Surprisingly, pathways related to NK cell-mediated toxicity were also enriched in our analyses (Figure 5C). These findings show that T cells, in which *Ezh2* is deleted, may possess unique features and share traits resembling NK cells. We refined our analysis by delineating a network of regulated genes encoding for proteins biophysically interacting with ≥2 other members. Two densely interconnected clusters were identified by MCODE (Molecular Complex Detection) algorithm and GO analysis on the network confirmed the significantly higher representation of terms related to NK cell-mediated toxicity and lymphocyte-mediated immunity (Figure 5D).

The prevalent enrichment of lymphocyte differentiation and NK cell pathways prompted an unbiased analysis of our results in the context of cell-specific transcriptional signatures. The most significant overlap of upregulated genes with cell identity in most murine atlases was NK cells rather than conventional T cell subtypes (Figure 5E). Notably, the differentially expressed genes overlapped with the variable genes in a scRNA-seq data set ([GSE152786] odds ratio, 14.3;  $P=2.4\times 10^{-13}$ ) of thymic iNKT cells.<sup>42</sup> This distinct T cell subset shows phenotypic and functional properties similar to NK cells and differentiates in the thymus under specific transcriptional programs driven by sequential transcription factors.<sup>43–45</sup> Hence, we analyzed the overlap between the transcription factors dictating iNKT development and the 29 transcription factors differentially regulated in our transcriptomic analysis, and found *Zbtb16* (zinc finger and BTB domain containing 16), the gene coding for Plzf (promyelocytic leukemia zinc finger), to be strongly upregulated in *Ezh2*-deficient CD4<sup>+</sup> T cells (Figure 5F). To assess the direct role of Ezh2 and the H3K27me3 mark in gene repression in T cells, we performed H3K27me3 ChIP on splenic CD3<sup>+</sup> T cells isolated from both Ezh2<sup>cd4</sup>-KO and Ezh2<sup>cd4</sup>-WT mice, followed by qPCR. This analysis revealed a significant enrichment of H3K27me3 at the transcription starting site of the *Zbtb16* gene in Ezh2<sup>cd4</sup>-WT mice, which was significantly diminished in Ezh2<sup>cd4</sup>-KO mice (Figure 5G). A similar pattern was observed for the *Il-4* gene (Figure 5G), reinforcing evidence for a lack of transcriptional repression of *Il-4* and

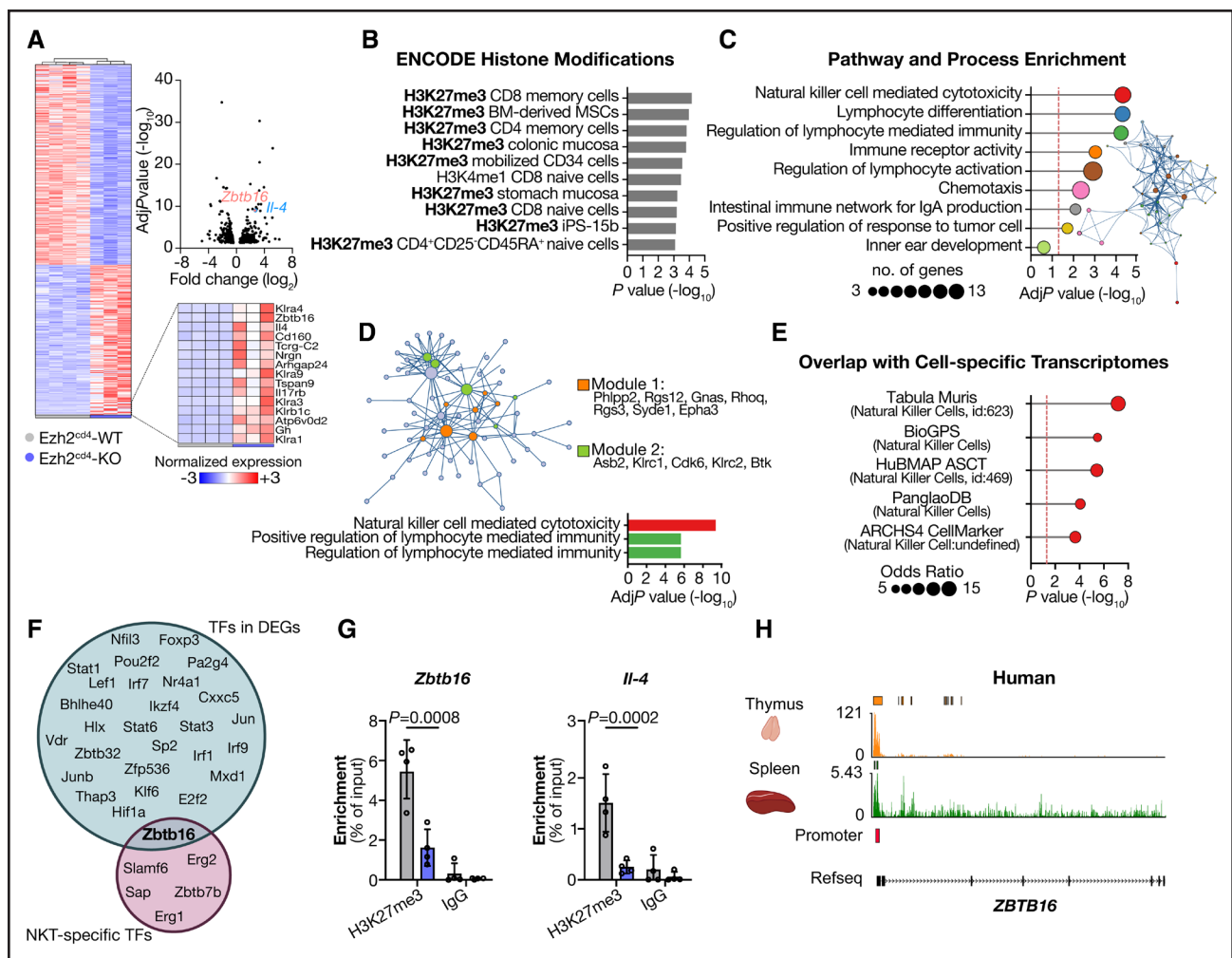


**Figure 5. Ezh2 deficiency in CD4<sup>+</sup> T cells epigenetically fosters the differentiation of iNKT cells.**

**A**, Differentially expressed genes (adjusted  $P$  value  $<0.05$ ) in CD4<sup>+</sup> T cells isolated from the spleen of atherosclerotic Ezh2<sup>cd4</sup>-WT and Ezh2<sup>cd4</sup>-KO mice ( $n=4$  vs 3). Gene expression is depicted in the heatmap, the top 15 upregulated genes are highlighted in the enlarged heatmap in the inset. Volcano plot reports  $P_{adj}$  values and fold changes as computed with edgeR. **B**, Enrichment analysis of upregulated genes in data sets of chromatin-immunoprecipitation (ChIP) sequencing of cells and tissues available from the epigenomics roadmap for histone modification in ENCODE. **C**, Pathway and process enrichment analysis for the upregulated genes in KEGG (Kyoto Encyclopedia of Genes and Genomes) pathways and Gene Ontology (GO) biological processes and molecular functions. The network of enriched terms is visualized with Cytoscape and color codes reflect the cluster IDs presented in the dot plot. **D**, Protein-to-protein interaction network of upregulated genes and GO enrichment analysis for the top three represented terms. The color defines the 2 densely interconnected clusters detected by Molecular Complex Detection and module components are enlisted. **E**, Overlap of the upregulated genes in CD4<sup>+</sup> T cells of Ezh2<sup>cd4</sup>-KO mice and available cell-specific transcriptomic data. For each atlas, the cell type with the most significant overlap (lowest  $P$  value, assessed by  $\chi^2$ ) is reported. **F**, Venn diagram showing the overlap between transcription factors (TF) significantly regulated in CD4<sup>+</sup> T cells of Ezh2<sup>cd4</sup>-KO mice and a list of TFs specific for iNKT cell development and differentiation described in the literature. **G**, ChIP-quantitative polymerase chain reaction analysis (qPCR) to analyze the enrichment of H3K27me3 and IgG control in splenic CD3<sup>+</sup> T cells at the promoter of *Zbtb16* (F) and *Il-4* (G) in Ezh2<sup>cd4</sup>-KO mice and respective controls ( $n=4$  vs 4). Data are represented as mean  $\pm$  SD. Comparisons were assessed using 2-way ANOVA test with multiple comparisons and Benjamini-Krieger-Yekutieli correction for false discovery rate (FDR) for **F** and **G**. **H**, Enrichment of H3K27me3 mark in the promoter of the *ZBTB16* gene in human thymus and spleen. Statistically significant peaks are noted above the read histograms. Data were retrieved from ENCODE ([Encyclopedia of DNA Elements] GSE18927 and GSE187334). *Akna* indicates AT-hook transcription factor; *Arhgap24*, rho GTPase activating protein 24; *Asb2*, ankyrin repeat and SOCS box-containing 2; *Atp6v0d2*, ATPase, H+ transporting, lysosomal V0 subunit D2; *Bhlhe40*, basic helix-loop-helix family, member e40; BM, bone marrow; *Bts*, zinc finger protein BRUTUS; CD, cluster of differentiation; *Cd160*, CD160 antigen; *Cdk6*, cyclin dependent kinase 6; *Cxnc5*, CXXC finger 5; DEG, differential expressed genes; *E2f2*, E2F transcription factor 2; *Epha3*, Eph receptor A3; *Erg1*, early growth response protein 1; *Erg2*, early growth response 2; *Ezh2*, enhancer of zeste homolog 2; *Foxp3*, forkhead box P3; *Gh*, growth hormone; *Gnas*, GNAS complex locus; H3K27me3, trimethylation of histone 3 lysine 27; *Hif1a*, hypoxia inducible factor 1, alpha subunit; *Hlx*, H2.0-like homeobox; IgG, Immunoglobulin G; *Ikzf4*, IKAROS family zinc finger 4; *Il17rb*, interleukin 17 receptor B; *Il4*, interleukin 4; iNKT, invariant natural killer T cells; *Irf1*, interferon regulatory factor 1; *Irf9*, interferon regulatory factor 9; *Jun*, jun proto-oncogene; *Junb*, jun B proto-oncogene; *Klf6*, kruppel-like transcription factor 6; *Klra1*, killer cell lectin-like receptor, subfamily A, member 1; *Klra3*, killer cell lectin-like receptor, subfamily A, member 3; *Klra4*, killer cell lectin-like receptor, subfamily A, member 4; *Klra9*, killer cell lectin-like receptor subfamily A, member 9; *Klrb1c*, killer cell lectin-like receptor subfamily B member 1C; *Klrc1*, killer cell lectin-like receptor subfamily C, member 1; *Klrc2*, killer cell lectin-like receptor subfamily C, member 2; KO, knockout; *Lef1*, (Continued)

**Figure 5 Continued.** lymphoid enhancer binding factor 1; *Mxd1*, MAX dimerization protein 1; *Nfil3*, nuclear factor interleukin 3 regulated; *Nr4a1*, nuclear receptor subfamily 4, group A, member 1; *Nrgn*, neurogranin; *Pa2g4*, proliferation-associated 2G4; *Phlpp2*, PH domain and leucine-rich repeat protein phosphatase 2; *Pou2f2*, POU domain, class 2, transcription factor 2; *Rgs12*, regulator of G-protein signaling 12; *Rgs3*, regulator of G-protein signaling 3; *Rhoq*, ras homolog family member Q; *Sap*, SLAM-associated protein; *Slamf6*, SLAM family member 6; *Sp2*, Sp2 transcription factor; *Stat1*, signal transducer and activator of transcription 1; *Stat3*, signal transducer and activator of transcription 3; *Stat6*, signal transducer and activator of transcription 6; *Syde1*, synapse defective 1, Rho GTPase, homolog 1; *Tcr $\gamma$ -C2*, T Cell Receptor Gamma Constant 2; *Thap3*, THAP domain containing, apoptosis-associated protein 3; *Tspan9*, tetraspanin 9; *Vdr*, vitamin D (1,25-dihydroxyvitamin D3) receptor; WT, wild type; *Zbtb16*, zinc finger and BTB domain containing 16; *Zbtb32*, zinc finger and BTB domain containing 32; *Zbtb7b*, zinc finger and BTB domain containing 7B; and *Zfp536*, zinc finger protein 536.

*Zbtb16* genes in the absence of H3K27me3 in *Ezh2<sup>cd4</sup>-KO* mice. Finally, we detected significant H3K27me3 enrichment at the regulatory promoter region of the *ZBTB16* gene in publicly available human ChIP-seq data (GSE18927 and GSE187334; Figure 5H), thus translating our findings on this EZH2-dependent regulatory pathway to humans. Together, our data suggest that EZH2 represses the transcriptional program, leading to iNKT differentiation by epigenetically repressing PLZF.

Our scRNA-seq data showed a strong increase in the fraction of iNKT cells in *Ezh2<sup>cd4</sup>-KO* mice (Figure 3D), which was validated by flow cytometry demonstrat-

ing a 3.8-fold increase in the iNKT cell proportion in the spleen of *Ezh2<sup>cd4</sup>-KO* mice (Figure 6A). iNKT cells are CD1d-restricted innate-like adaptive lymphocytes capable of responding quickly (ie, minutes to hours) on antigenic lipid stimulation.<sup>46</sup> Analogous to conventional T cells, iNKT cells differentiate into distinct subsets, namely iNKT1, iNKT2, and iNKT17 cells.<sup>47</sup> More detailed analysis revealed that splenic iNKT cells of *Ezh2<sup>cd4</sup>-KO* mice strongly express *Plzf*, the hallmark of iNKT2 cells (Figure 6B). Further phenotyping confirmed a striking shift from iNKT1 cells in *Ezh2<sup>cd4</sup>-WT* mice toward *Plzf*-expressing iNKT2 cells in *Ezh2<sup>cd4</sup>-KO* mice (Figure 6C;

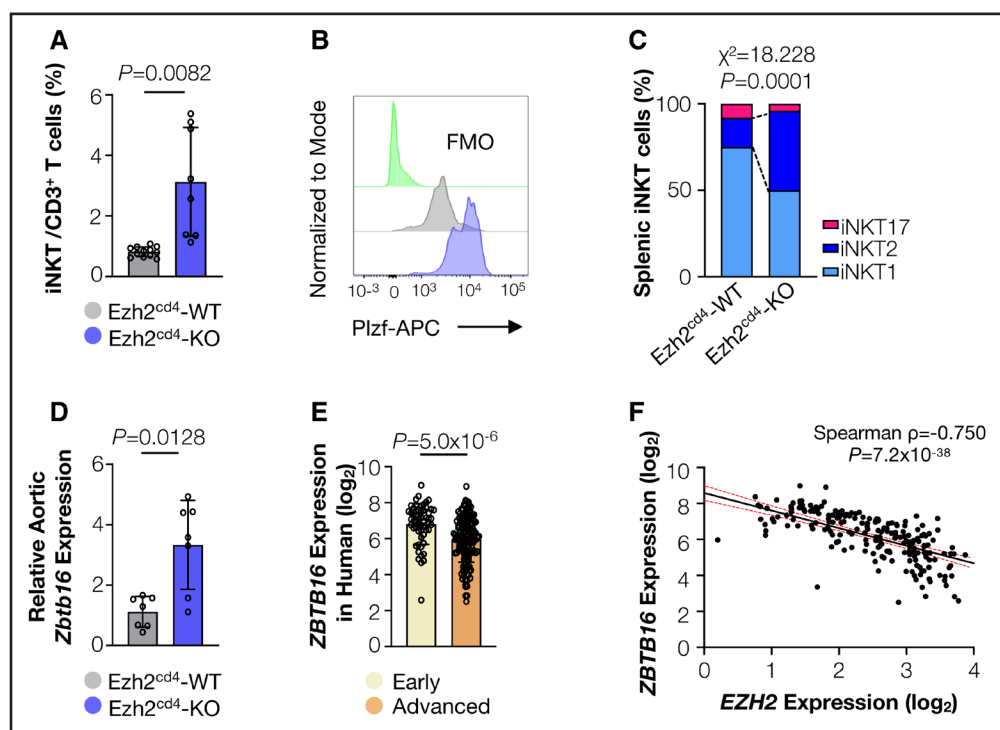


**Figure 6. Accumulation of iNKT2 cells in *Ezh2<sup>cd4</sup>-KO* mice.**

**A**, Flow cytometric (FC) analysis of splenic iNKT cells (CD1d<sup>+</sup>TCR $\beta$ <sup>+</sup>) from atherosclerotic *Ezh2<sup>cd4</sup>-WT* and *Ezh2<sup>cd4</sup>-KO* mice (n=12 vs 8). **B**, Representative FC histogram displaying the comparison of *Plzf* (promyelocytic leukemia zinc finger) protein expression in iNKT cells from both mouse strains and fluorescence minus one (FMO) control. **C**, Splenic iNKT comparison between *Ezh2<sup>cd4</sup>-WT* and *Ezh2<sup>cd4</sup>-KO* mice and classification into iNKT1 (*Plzf<sup>low</sup>*), iNKT2 (*Plzf<sup>high</sup>*), and iNKT17 (*Plzf<sup>interm</sup>*; ROR $\gamma$ t<sup>+</sup>) subsets (n=5 vs 6). **D**, Gene expression of *Zbtb16* in the descending aorta of atherosclerotic *Ezh2<sup>cd4</sup>-WT* and *Ezh2<sup>cd4</sup>-KO* mice measured by quantitative polymerase chain reaction (n=7 vs 7). **E**, *ZBTB16* expression in advanced atherosclerotic plaques vs early lesions from bulk RNA-sequencing data of human carotid endarterectomy (CEA) samples of the Munich Vascular Biobank. **F**, Bivariate correlation between *ZBTB16* (y-axis) and *EZH2* (x-axis) in human atherosclerotic plaques from the Munich Vascular Biobank visualized as a linear regression line with 95% CI. Data are represented as mean $\pm$ SD; comparisons were assessed by 2-tailed Student *t* test with Welch's correction (**A**),  $\chi^2$  distribution analysis (**C**), 2-tailed Mann-Whitney *U* test (**D** and **E**), and Spearman correlation test (**F**). APC indicates allophycocyanin; CD, cluster of differentiation; *Ezh2*, enhancer of zeste homolog 2; iNKT, invariant natural killer T cells; KO, knockout; ROR $\gamma$ t, retinoic acid-related orphan receptor  $\gamma$ t; TCR $\beta$ , T cell receptor  $\beta$ ; WT, wild type; and *ZBTB16*, zinc finger and BTB domain containing 16.

Figure S6A). This suggests that in the absence of T cell-specific *Ezh2*, iNKT cells are not only vastly expanded, but also preferentially differentiate toward an iNKT2 phenotype. Likewise, the expression of *Zbtb16* was significantly upregulated in atherosclerotic aortas of *Ezh2<sup>cd4</sup>-KO* mice (Figure 6D), indicating that Plzf-expressing iNKT2 cells accumulate in atherosclerotic plaques on *Ezh2* deletion in T cells. This finding aligns with the 2.0-fold decrease of *ZBTB16* expression in human advanced versus early lesions ( $P=2.1\times 10^{-6}$ ) in the Munich Vascular Biobank with a high-grade negative bivariate correlation with *EZH2* expression (Spearman  $\rho=-0.750$ ;  $P=7.2\times 10^{-38}$ ; Figure 6E and 6F), suggesting that the atheroprotective role of ZBTB16 and iNKT2 cells is translatable to humans. Notably, iNKT populations and Plzf expression in the spleen of *Ezh2<sup>cd8</sup>-KO* mice were similar to their WT littermates (Figure S5J), supporting our finding that the effects observed are attributable to *Ezh2* deficiency in  $CD4^+$ - and not  $CD8^+$ -T cells.

## Thymic iNKT2 Cells in *Ezh2<sup>cd4</sup>-KO* Mice Initiate Type 2 Immune Responses

Similar to conventional T cell populations, iNKT cells originate from  $CD4^+/CD8^+$  double-positive precursors in the thymus. In contrast to conventional T cells that differentiate in the periphery, iNKT cells differentiate in the thymus into functionally distinct iNKT1, iNKT2, or iNKT17 subsets.<sup>48</sup> Contrary to the significant decreases in T cell numbers in the circulation and secondary lymphoid organs of *Ezh2<sup>cd4</sup>-KO* mice (Figure 3A and 3B), we observed a massive accumulation of  $CD3^+$  T cells in the thymus of *Ezh2<sup>cd4</sup>-KO* mice (Figure 7A), which could be ascribed to differences in the thymic development of T cells. We observed a reduction in the proportion of double-positive cells (Figure 7B), along with an accumulation of double-negative 1 and 4 populations (Figure 7C), leading to a profound decrease in thymic  $CD4^+$  T cells in *Ezh2<sup>cd4</sup>-KO* mice, whereas thymic  $CD8^+$  T cells were

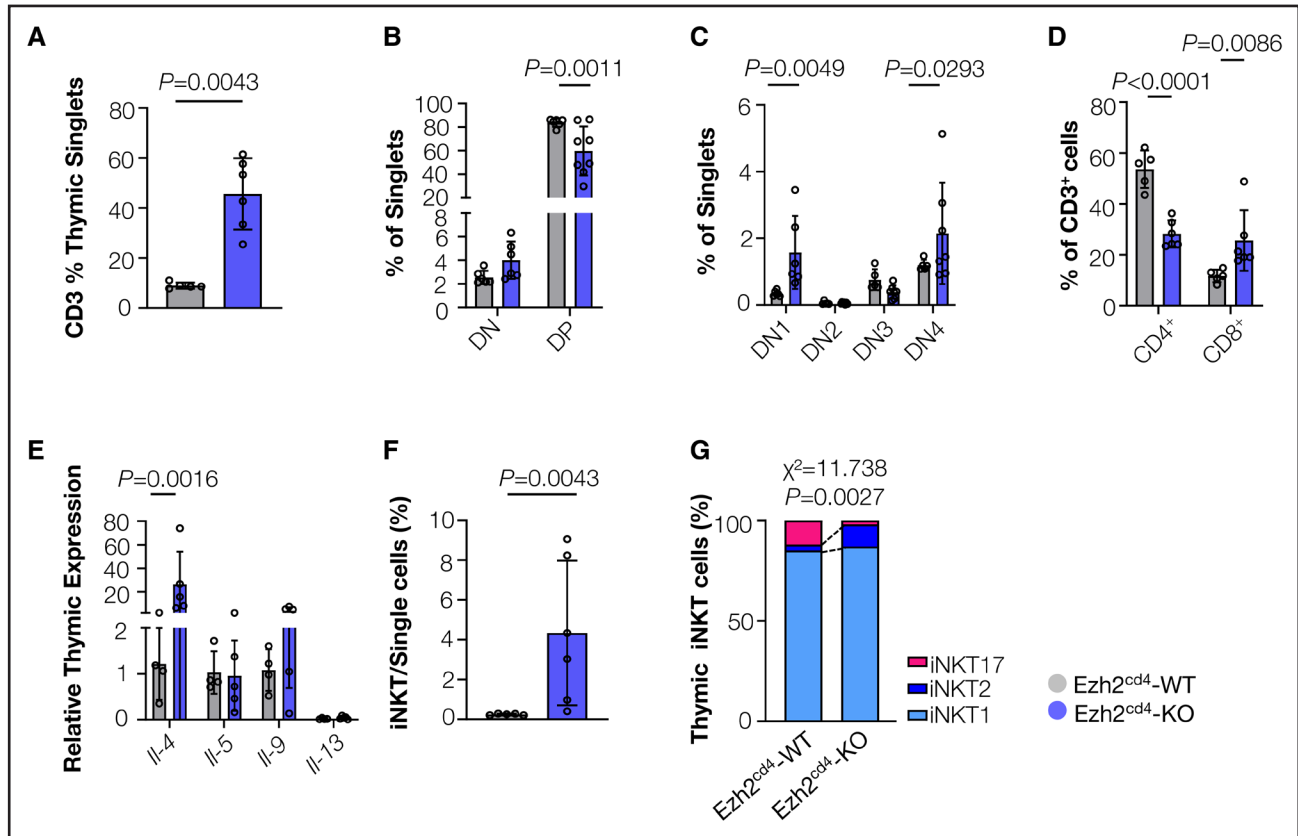


**Figure 7. Thymic iNKT2 cells in *Ezh2<sup>cd4</sup>-KO* mice initiate the type 2 immune response.**

**A**, Flow cytometric (FC) analysis of thymic  $CD3^+$  T cells from atherosclerotic *Ezh2<sup>cd4</sup>-WT* and *Ezh2<sup>cd4</sup>-KO* mice ( $n=5$  vs 6). **B**, FC analysis of thymocytes from atherosclerotic *Ezh2<sup>cd4</sup>-WT* and *Ezh2<sup>cd4</sup>-KO* mice to identify double negative (DN) and double positive (DP) subsets ( $n=6$  vs 6–8). **C**, Proportion of DN subsets was determined based on  $CD44$  and  $CD25$  expression. DN1 ( $CD44^+/CD25^+$ ), DN2 ( $CD44^+/CD25^+$ ), DN3 ( $CD44^+/CD25^+$ ), and DN4 ( $CD44^+/CD25^+$ ). **D**, FC analysis of thymic  $CD4^+$  T and  $CD8^+$  T cells from atherosclerotic *Ezh2<sup>cd4</sup>-WT* and *Ezh2<sup>cd4</sup>-KO* mice ( $n=5$ –6 vs 6–7). **E**, Gene expression of *Il-4*, *Il-5*, *Il-9*, and *Il-13* (interleukins 4, 5, 9, and 13, respectively) in the thymus of atherosclerotic *Ezh2<sup>cd4</sup>-WT* and *Ezh2<sup>cd4</sup>-KO* mice ( $n=5$  vs 6). **F**, FC analysis of thymic iNKT cells ( $CD1d^+TCR\beta^+$ ) from atherosclerotic *Ezh2<sup>cd4</sup>-WT* and *Ezh2<sup>cd4</sup>-KO* mice ( $n=5$  vs 6). **G**, Comparison of thymic iNKT cells ( $CD1d^+TCR\beta^+$ ) from *Ezh2<sup>cd4</sup>-WT* and *Ezh2<sup>cd4</sup>-KO* mice and subclassification into iNKT1 (Plzf<sup>low</sup>), iNKT2 (Plzf<sup>high</sup>) and iNKT17 (Plzf<sup>interm</sup>, ROR $\gamma$ t<sup>+</sup>) subsets ( $n=5$  vs 6). Data are represented as mean $\pm$ SD; comparisons were assessed by 2-tailed Mann-Whitney *U* test (**A** and **F**), 2-way ANOVA with multiple comparisons and Benjamini-Krieger-Yekutieli correction for false discovery rate (**B** through **E**), and  $\chi^2$  distribution analysis (**G**). CD indicates cluster of differentiation; *Ezh2*, enhancer of zeste homolog 2; iNKT, invariant natural killer T cells; KO, knockout; Plzf, promyelocytic leukemia zinc finger; ROR $\gamma$ t, retinoic acid–related orphan receptor  $\gamma$ ; TCR $\beta$ , T cell receptor  $\beta$ , and WT, wild type.

only slightly increased (Figure 7D). *Foxp3* expression was barely detectable in the thymus of *Ezh2<sup>cd4</sup>-KO* mice (Figure S6D), indicating that the profound reduction of systemic and lesional Tregs can be attributed to the disturbed T cell development in the thymus. To unravel the source of the type 2 immune response in *Ezh2<sup>cd4</sup>-KO* mice, we examined the cytokine milieu in the thymus. In parallel to the periphery, we observed a profound increase in *Il-4* transcripts and iNKT cells in the thymus of *Ezh2<sup>cd4</sup>-KO* mice (Figure 7E and 7F). Corroborating our findings in the spleen, *Ezh2* deficiency in CD4<sup>+</sup> T cells skewed the iNKT cells toward an iNKT2 phenotype (Figure 7G; Figure S6B), which likely explains the increase in *Il-4* in the thymus.

Overall, our data suggest that the increased abundance of iNKT2 cells in the thymus of *Ezh2<sup>cd4</sup>-KO* mice is the source of *Il-4* and a driving force for the type 2 immune response and subsequent CD4<sup>+</sup> and CD8<sup>+</sup> T cell polarization in the periphery and atherosclerotic aorta.

### Noncanonical Function of Ezh2 in T Cells in Atherosclerosis

To discriminate between the canonical and potential noncanonical, chromatin-independent role of EZH2 in the context of atherosclerosis, we investigated the cellular localization of EZH2 in T cells in atherosclerotic lesions using immunofluorescence staining. In both murine and human plaque specimens, we mainly observed the presence of EZH2 in the nucleus. However, we could confirm weak expression of EZH2 in the cytoplasm of lesional T cells (Figure 8A and 8B). These findings suggest mainly canonical (chromatin-dependent), but also noncanonical activity of EZH2 in T cells in human and mouse atherosclerotic plaques.

Previous studies found that *Ezh2* controls actin polymerization,<sup>49</sup> cell adhesion, and migration through direct methylation of extranuclear substrates.<sup>28</sup> In support of these reports, we could demonstrate a profound reduction in actin filaments in CD4<sup>+</sup> T cells isolated from *Ezh2<sup>cd4</sup>-KO* mice (Figure 8C). Moreover, we observed a strong impairment in the migratory capacity of these *Ezh2*-deficient CD4<sup>+</sup> T cells toward the chemokines Ccl19 and Ccl22, compared with CD4<sup>+</sup> T cells from *Ezh2<sup>cd4</sup>-WT* mice (Figure 8D). Altogether, our data suggest an additional noncanonical, chromatin-independent function of *Ezh2* in T cells, likely contributing to attenuated atherosclerosis in *Ezh2<sup>cd4</sup>-KO* mice.

## DISCUSSION

Our study demonstrates that T cell *Ezh2* deficiency in atherosclerosis leads to systemic and local increases of the type 2 cytokines, which drive iNKT2, Th2, and anti-inflammatory macrophage polarization, and limits atherosclerosis progression.

Unlike the unambiguous, pro-atherogenic role of IFN- $\gamma$ -producing Th1 cells,<sup>50–52</sup> the role of T cells producing type 2 cytokines in atherosclerosis remains controversial. Early studies suggested that *Il-4* was either pro-atherogenic or not involved in the induction of atherosclerosis.<sup>53,54</sup> Conversely, *Il-13* was reported to reduce atherogenesis, promoting polarization of alternatively activated macrophages.<sup>55</sup> However, dissecting individual contributions of *Il-4* and *Il-13* is complicated by sharing a common receptor (ie, *Il-4* receptor), leading to tyrosine phosphorylation of STAT6 (signal transducer and activator of transcription 6), a transcriptional regulator of Th2 cells and macrophages crucial for atherosclerosis regression.<sup>56,57</sup> Mice deficient in both *Il-4* and *Il-13* were found to be resistant to plaque regression after ApoB silencing, suggesting both cytokines are key players in resolving macrophage-induced inflammation through elevated expression of pro-resolving genes, such as *Arg1* and *Socs1* (suppressor of cytokine signaling 1).<sup>58</sup>

Production of *Il-4* and *Il-13* is predominantly associated with Th2 cells, but innate and innate-like immune cells such as iNKTs, mast cells, and eosinophils can also produce type 2 cytokines. Likewise, our analyses indicate that T cell *Ezh2* deficiency in mice promotes the differentiation toward iNKT cells. Intriguingly, we demonstrate that this switch was triggered by the transcriptional regulation of the specific transcription factor *Zbtb16*. Although we identified a significant overlap between the upregulated genes and published data set of iNKT cells (GSE152786), our analysis did not prominently feature iNKT pathways and an enrichment (39-fold) could only be observed for GO term positive regulation of NK T cell differentiation (GO:0051138), without retaining statistical significance upon false discovery rate. This most likely reflects the distinctly overlapping signature between T, NK, and iNKT cell transcriptomes, as evidenced by a recent scRNA-seq data set<sup>43</sup> and the lack of GO terms specifically featuring iNKT cells.

iNKT cells are innate-like CD4<sup>+</sup> or double-negative CD4<sup>-</sup>/CD8<sup>-</sup> T cells, which respond quickly on stimulation by glycolipids, instead of peptides, presented by the major histocompatibility class I molecule CD1d.<sup>48</sup> iNKT cells develop in the thymus, where they immediately diverge into functionally distinct iNKT1, iNKT2, and iNKT17 subsets, defined by the transcription factors PLZF, Tbx21 ([Tbet] T-box 21), GATA-3 (GATA-binding protein 3), and ROR $\gamma$ t (retinoic acid-related orphan receptor  $\gamma$ t), respectively, and by the release of T helper-associated cytokines including IFN- $\gamma$ , *Il-4*, and *Il-17A*.<sup>59,60</sup> To date, the contribution of iNKT cells to the development of atherosclerosis remains ambiguous. Initial studies indicate mice deficient in iNKT cells displayed lower atherosclerotic plaque burden and inhibition of iNKT activation using CD1d antagonists could attenuate established atherosclerosis.<sup>61,62</sup> However, both studies neglected the individual contributions of iNKT subsets,



which may exert pro- and anti-atherogenic effects. In *Ezh2<sup>cd4</sup>-KO* mice, we observed a high expression of *Plzf* in the expanded iNKT population, which is associated with iNKT2 cells that predominantly secrete IL-4.<sup>60</sup> The expansion of *Plzf<sup>high</sup>* iNKT2 cells already occurred in the thymus of *Ezh2<sup>cd4</sup>-KO* mice, indeed accompanied by an enrichment in IL-4. Previous studies have shown that local IL-4 within the thymic environment can polarize CD8<sup>+</sup> T cells toward an innate-memory phenotype, which then drive dendritic cells to secrete *Ccl17* and *Ccl22* and thereby to inhibit thymic export of T cells into peripheral tissues.<sup>47</sup> These chemokines interact with *Ccr4*, which is expressed on iNKT2 cells, fueling a positive feedback loop.<sup>63</sup> *Ezh2<sup>cd4</sup>-KO* mice indeed showed a CD8<sup>+</sup> T cell shift toward an innate-memory phenotype, accompanied by elevated *Ccl17* transcript levels in the thymus (Figure S6C), and subsequently a reduction in CD4<sup>+</sup> T cells, both in the circulation and in the periphery. The fact that this phenotype could not be reproduced in a CD8<sup>+</sup>-specific *Ezh2*-knockout (KO) model underscores the role of IL-4 (and IL-13) as the driving force behind this effect.

A study with mice lacking both *Ezh2* and iNKT cell populations demonstrated that IL-4 and IL-13 production did not originate from peripheral T cells but from iNKT2 cells,<sup>23</sup> which ultimately polarize CD4<sup>+</sup> T cells toward a Th2 phenotype and induce additional type 2 cytokine secretion. We confirmed these findings, given the profound increase in iNKT2 cells along with enhanced IL-4 in the thymus, whereas the CD4<sup>+</sup> T cell shift toward a Th2 phenotype was only observed in the periphery.

iNKT cells are also present in the periphery and display committed tissue-residency, notably after lineage commitment in the thymus.<sup>48,64</sup> Although long-term residency in the liver, spleen, and lymph nodes has been established for iNKT1 cells,<sup>65</sup> insights into iNKT2 tissue localization and residency remain elusive. Interestingly, in our *Ezh2<sup>cd4</sup>-KO* mice, *Zbtb16*, the gene coding for *Plzf*, and *Il-4* transcripts were increased in the aorta, suggesting—on top of the expansion of iNKT2 cells in the thymus and spleen—local enrichment of IL-4-producing *Plzf<sup>high</sup>* iNKT2 cells. Although the notorious difficulties in resolving T cell subsets by scRNA-seq limited our ability to identify an iNKT2 cell cluster in human atherosclerotic plaques, the lower *ZBTB16* expression in advanced vs early lesions detected by bulk RNAseq serves as a proxy for lower prevalence of this iNKT2 cell subset and confers translational perspective of our findings.

Mechanistically, 2 different ways for EZH2-mediated PLZF regulation have been proposed. In a more traditional role, EZH2 represses the expression of multiple transcription factors and downstream genes by lowering chromatin accessibility.<sup>23</sup> We confirmed this hypothesis in splenic T cells from our mice using H3K27me3 ChIP-qPCR, indicating that *Ezh2* represses the transcriptional program leading to iNKT2 differentiation by epigenetically repressing *Plzf*. In a noncanonical way, however,

EZH2 can directly methylate PLZF leading to its ubiquitination and degradation.<sup>27</sup> Moreover, it has been shown that extra-nuclear action of *Ezh2* compromises migratory capacity of dendritic cells by impairing the interaction of talin and F-actin.<sup>28</sup> In *Ezh2<sup>cd4</sup>-KO* mice, actin filaments and the migratory capacity of CD4<sup>+</sup> T cells were profoundly reduced, likely delaying atherosclerosis progression. Altogether, altered gene expression and disturbed actin polymerization may account for the observed iNKT2 phenotype and the subsequent athero-protection.

Interestingly, T cell-specific *Ezh2* deficiency also affected Tregs. *Foxp3* acts as a transcriptional repressive mark allowing a physical interaction with EZH2 to target genes for H3K27me3 repression.<sup>66</sup> Furthermore, defective induction of *Foxp3* expression can be a result of overstimulation from T helper cytokines, including IL-4.<sup>67</sup> Likewise, thymic *Foxp3* was profoundly suppressed in *Ezh2<sup>cd4</sup>-KO* mice. Although Tregs are generally viewed as powerful anti-inflammatory mediators,<sup>68</sup> previous murine atherosclerosis studies revealed that Tregs are protective at the early disease stages but only play a minor role in advanced atherosclerosis.<sup>69</sup> Notably, the primary anti-inflammatory cytokines produced by Tregs, namely Tgf- $\beta$  and IL-10 were not diminished in *Ezh2<sup>cd4</sup>-KO* mice (Figure S6E). Overall, the type 2 immune response observed in *Ezh2<sup>cd4</sup>-KO* mice seems sufficient to resolve inflammation independently of Tregs.

Recent studies indicated that pharmacological inhibition of *Ezh2* can reduce atherosclerosis potentially without an involvement of T cells. Administration of an *Ezh2* inhibitor, GSK126, in atherosclerotic *ApoE<sup>-/-</sup>* mice delayed plaque progression by reducing monocyte recruitment.<sup>70</sup> However, effects of GSK126 on T cell phenotype and function were not studied, a gap that should be addressed. Another mouse study has demonstrated a significant role of myeloid-*Ezh2* in atherogenesis,<sup>71</sup> likely suggesting a synergistic role of T cell- and myeloid *Ezh2*. Nonetheless, our human data point to higher expression of EZH2 in T cell clusters, suggesting expression within lymphocytes may be a more appropriate translational target. Notably, the US Food and Drug Administration granted first-in-class accelerated approval of the EZH2 inhibitor tazemetostat for neoplastic diseases,<sup>72,73</sup> confirming the feasibility of EZH2 inhibition in clinical practice. This paves the way for future clinical trials repurposing EZH2 inhibitors for treating atherosclerotic cardiovascular disease.

Taken together, our data identify EZH2 as a main player in T cell differentiation and activation by suppressing anti-atherogenic type 2 cytokine production initiated by iNKT2 cells, thereby establishing a promising immunotherapeutic target in atherosclerosis.

## ARTICLE INFORMATION

Received September 24, 2024; accepted December 16, 2024.

## Affiliations

Institute for Cardiovascular Prevention (C.A.B., M.L., V.T., F.M.F., K.N., Y.W., V.B., I.A.-K., Y.F.S.M., M.K., K.R., C.W., D.S., E.L., D.A.); Anthropology and Human Genetics, Faculty of Biology (A.J., W.E.); Institute of Informatics (M.J.); Department of Molecular Biology (A.V.V., A.I.) and Protein Analysis Unit (A.I.), Biomedical Center Munich, Faculty of Medicine; Graduate School of Quantitative Biosciences (A.V.V.); and Walter Straub Institute of Pharmacology and Toxicology (D.A.), Ludwig Maximilians Universität, Munich, Germany. DZHK (German Center for Cardiovascular Research), Partner Site Munich Heart Alliance, Germany (C.A.B., F.M.F., V.B., I.A.-K., M.K., L.M., C.W., D.S., E.L., D.A.). Department of Medical Laboratory Sciences, Virginia Commonwealth University, Richmond (M.L.). Department of Cardiovascular Medicine and Immunology, Mayo Clinic, Rochester, MN, (K.N., E.L.). Institute of Molecular Vascular Medicine, Technical University Munich, Klinikum Rechts der Isar, Germany; (L.M.). Molecular Vascular Medicine Unit, Department of Medicine, Karolinska Institutet, Stockholm, Sweden (L.M.). Department of Medical Biochemistry, Amsterdam Institute for Cardiovascular Sciences, Atherosclerosis and Ischemic Syndromes, Amsterdam Institute for Infection and Immunity, Inflammatory Diseases, Amsterdam University Medical Center, The Netherlands (M.d.W.). Munich Cluster for Systems Neurology (SyNergy), Germany (C.W.). Institute for Genetic and Biomedical Research, Unit of Milan, National Research Council, Italy (D.S.).

## Acknowledgments

The authors would like to acknowledge Sigrid Unterlugauer, Linda Beckers, and Myrthe de Toom for their excellent histological skills. They would also like to acknowledge Yvonne Jansen for her invaluable dissection skills. Brilliant violet–conjugated tetramers of CD1d were generously provided by the Tetramer Core Facility of the US National Institutes of Health. The authors thank Dr Stuart Orkin, Boston Children's Hospital for us providing the Ezh2-flox mice and Prof Dr Andreas Thiel, Berlin Institute of Health at Charité Berlin for us gifting the CD8cre mice.

## Sources of Funding

This study was supported by the Deutsche Forschungsgemeinschaft (DFG 671836 to D.A., CRC 1123 to A.I., L.M., D.S., D.A., E.L., W.E., and C.W.; 403584255-TRR 267-A02 to C.W.). The authors also acknowledge the support from the Netherlands CardioVascular Research Initiative: the Dutch Heart Foundation, Dutch Federation of University Medical Centers, the Netherlands Organization for Health Research and Development and the Royal Netherlands Academy of Sciences for the GENIUS-II project "Generating the best evidence-based pharmaceutical targets for Atherosclerosis" [CVON2017-20]. This study was also supported by the EU (Horizon 2020, REPROGRAM to E.L. and M.d.W.); the German Centre for Cardiovascular Research (DZHK) [TRP grant to E.L., D.A. and C.W., Shared expertise grant to M.L., D.A., Women scientist grant to D.A.; projects 81X2600269 and 81Z0600203 to D.S.], the Bundesministerium für Bildung und Forschung (BMBF) and Free State of Bavaria (LMU Excellence strategy to C.W. and D.S.), and the European Research Council [ERC consolidator grant to E.L., ERC advanced grant 692511 to C.W.], E.L. is supported by the Leducq foundation (CHECKPOINT ATHERO network of excellence grant). MdW is supported by the Netherlands Heart Foundation (CVON 2017-20); the Netherlands Heart Foundation and Spark-Holding BV (2019B016); Leducq Foundation (LEAN Transatlantic Network Grant, 16CVD01); Amsterdam UMC; Amsterdam Cardiovascular Sciences; ZonMW (Open competition 09120011910025). C.W. is a Van der Laar Professor of atherosclerosis.

## Disclosures

None.

## Supplemental Material

Supplemental Methods

Figures S1–S7

Tables S1–S7

References 74–96

## REFERENCES

- Libby P. The changing landscape of atherosclerosis. *Nature*. 2021;592:524–533. doi: 10.1038/s41586-021-03392-8
- Weber C, Habenicht AJR, von Hundelshausen P. Novel mechanisms and therapeutic targets in atherosclerosis: inflammation and beyond. *Eur Heart J*. 2023;44:2672–2681. doi: 10.1093/eurheartj/ehad304

- de Winther RPJ, Bäck M, Evans P, Gomez D, Goncalves I, Jørgensen HF, Koenen RR, Lutgens E, Norata GD, Osto E, et al. Translational opportunities of single-cell biology in atherosclerosis. *Eur Heart J*. 2023;44:1216–1230. doi: 10.1093/eurheartj/ehac686
- Engelen SE, Robinson AJB, Zurke YX, Monaco C. Therapeutic strategies targeting inflammation and immunity in atherosclerosis: how to proceed? *Nat Rev Cardiol*. 2022;19:522–542. doi: 10.1038/s41569-021-00668-4
- Fernandez DM, Rahman AH, Fernandez NF, Chudnovskiy A, Amir ED, Amadori L, Khan NS, Wong CK, Shamailova R, Hill CA, et al. Single-cell immune landscape of human atherosclerotic plaques. *Nat Med*. 2019;25:1576–1588. doi: 10.1038/s41591-019-0590-4
- Depuydt MAC, Schaftenaar FH, Prange KHM, Boltjes A, Hemme E, Delfos L, de Mol J, de Jong MJM, Bernabé Kleijn MNA, Peeters JAHM, et al. Single-cell T cell receptor sequencing of paired human atherosclerotic plaques and blood reveals autoimmune-like features of expanded effector T cells. *Nat Cardiovasc Res*. 2023;2:112–125. doi: 10.1038/s44161-022-00208-4
- Dib L, Koneva LA, Edsfeldt A, Zurke YX, Sun J, Nitulescu M, Attar M, Lutgens E, Schmidt S, Lindholm MW, et al. Lipid-associated macrophages transition to an inflammatory state in human atherosclerosis, increasing the risk of cerebrovascular complications. *Nat Cardiovasc Res*. 2023;2:656–672. doi: 10.1038/s44161-023-00295-x
- Wang Z, Zhang X, Lu S, Zhang C, Ma Z, Su R, Li Y, Sun T, Li Y, Hong M, et al. Pairing of single-cell RNA analysis and T cell antigen receptor profiling indicates breakdown of T cell tolerance checkpoints in atherosclerosis. *Nat Cardiovasc Res*. 2023;2:290–306. doi: 10.1038/s44161-023-00218-w
- Saigusa R, Roy P, Freuchet A, Gulati R, Ghosheh Y, Suthahar SA, Durant CP, Hanna DB, Kioussis WB, Orecchioni M, et al. Single cell transcriptomics and TCR reconstruction reveal CD4 T cell response to MHC-II-restricted APOB epitope in human cardiovascular disease. *Nat Cardiovasc Res*. 2022;1:462–475. doi: 10.1038/s44161-022-00063-3
- Durek P, Nordström K, Gasparoni G, Salhab A, Kressler C, de Almeida M, Bassler K, Ulas T, Schmidt F, Xiong J, et al; DEEP Consortium. Epigenomic profiling of human CD4+ T cells supports a linear differentiation model and highlights molecular regulators of memory development. *Immunity*. 2016;45:1148–1161. doi: 10.1016/j.immuni.2016.10.022
- Wang Z, Yin H, Lau CS, Lu O. Histone posttranslational modifications of CD4+ T cell in autoimmune diseases. *Int J Mol Sci*. 2016;17:1–16. doi: 10.3390/ijms17101547
- Rodriguez RM, Lopez-Larrea C, Suarez-Alvarez B. Epigenetic dynamics during CD4+ T cells lineage commitment. *Int J Biochem Cell Biol*. 2015;67:75–85. doi: 10.1016/j.biocel.2015.04.020
- Wei G, Wei L, Zhu J, Zang C, Hu-Li J, Yao Z, Cui K, Kanno Y, Roh TY, Watford WT, et al. Global mapping of H3K4me3 and H3K27me3 reveals specificity and plasticity in lineage fate determination of differentiating CD4+ T cells. *Immunity*. 2009;30:155–167. doi: 10.1016/j.immuni.2008.12.009
- Blackledge NP, Klose RJ. The molecular principles of gene regulation by polycomb repressive complexes. *Nat Rev Mol Cell Biol*. 2021;22:815–833. doi: 10.1038/s41580-021-00398-y
- Schuettengruber B, Chourrout D, Vervoort M, Leblanc B, Cavalli G. Genome regulation by polycomb and trithorax proteins. *Cell*. 2007;128:735–745. doi: 10.1016/j.cell.2007.02.009
- Müller J, Hart CM, Francis NJ, Vargas ML, Sengupta A, Wild B, Miller EL, O'Connor MB, Kingston RE, Simon JA. Histone methyltransferase activity of a Drosophila Polycomb group repressor complex. *Cell*. 2002;111:197–208. doi: 10.1016/s0092-8674(02)00976-5
- Kuzmichev A, Nishioka K, Erdjument-Bromage H, Tempst P, Reinberg D. Histone methyltransferase activity associated with a human multiprotein complex containing the enhancer of zeste protein. *Genes Dev*. 2002;16:2893–2905. doi: 10.1101/gad.1035902
- Agger K, Cloos PAC, Christensen J, Pasini D, Rose S, Rappsilber J, Issaeva I, Canaan E, Salcini AE, Helin K. UTX and JMJD3 are histone H3K27 demethylases involved in HOX gene regulation and development. *Nature*. 2007;449:731–734. doi: 10.1038/nature06145
- De Santa F, Totaro MG, Prosperini E, Notarbartolo S, Testa G, Natoli G. The histone H3 lysine-27 demethylase Jmjd3 links inflammation to inhibition of polycomb-mediated gene silencing. *Cell*. 2007;130:1083–1094. doi: 10.1016/j.cell.2007.08.019
- Dobenecker MW, Park JS, Marcello J, McCabe MT, Gregory R, Knight SD, Rioja I, Bassil AK, Prinjha RK, Tarakhovskiy A. Signaling function of PRC2 is essential for TCR-driven T cell responses. *J Exp Med*. 2018;215:1101–1113. doi: 10.1084/jem.20170084
- Neele AE, de Winther RPJ. Repressing the repressor: Ezh2 mediates macrophage activation. *J Exp Med*. 2018;215:1269–1271. doi: 10.1084/jem.20180479

22. Zhang X, Wang Y, Yuan J, Li N, Pei S, Xu J, Luo X, Mao C, Liu J, Yu T, et al. Macrophage/microglial Ezh2 facilitates autoimmune inflammation through inhibition of Socs3. *J Exp Med*. 2018;215:1365–1382. doi: 10.1084/jem.20171417
23. Tumes D, Hirahara K, Papadopoulos M, Shinoda K, Onodera A, Kumagai J, Yip KH, Pant H, Kokubo K, Kiuchi M, et al. Ezh2 controls development of natural killer T cells, which cause spontaneous asthma-like pathology. *J Allergy Clin Immunol*. 2019;144:549–560.e10. doi: 10.1016/j.jaci.2019.02.024
24. Tumes DJ, Onodera A, Suzuki A, Shinoda K, Endo Y, Iwamura C, Hosokawa H, Koseki H, Tokoyoda K, Suzuki Y, et al. The [oligocomb protein Ezh2 regulates differentiation and plasticity of CD4+ T helper type 1 and type 2 cells. *Immunity*. 2013;39:819–832. doi: 10.1016/j.immuni.2013.09.012
25. Li F, Zeng Z, Xing S, Gullicksrud JA, Shan Q, Choi J, Badovinac VP, Crotty S, Peng W, Xue HH. Ezh2 programs T FH differentiation by integrating phosphorylation-dependent activation of Bcl6 and polycomb-dependent repression of p19Arf. *Nat Commun*. 2018;9:5452. doi: 10.1038/s41467-018-07853-z
26. Araki Y, Wang Z, Zang C, Wood WH, Schones D, Cui K, Roh TY, Lhotsky B, Wersto RP, Peng W, et al. Genome-wide analysis of histone methylation reveals chromatin state-based regulation of gene transcription and function of memory CD8+ T cells. *Immunity*. 2009;30:912–925. doi: 10.1016/j.immuni.2009.05.006
27. Vasanthakumar A, Xu D, Lun AT, Kueh AJ, van Gisbergen KP, Iannarella N, Li X, Yu L, Wang D, Williams BR, et al. A non-canonical function of Ezh2 preserves immune homeostasis. *EMBO Rep*. 2017;18:619–631. doi: 10.15252/embr.201643237
28. Gunawan M, Venkatesan N, Loh JT, Wong JF, Berger H, Neo WH, Li LYJ, La Win MK, Yau YH, Guo T, et al. The methyltransferase Ezh2 controls cell adhesion and migration through direct methylation of the extranuclear regulatory protein talin. *Nat Immunol*. 2015;16:505–516. doi: 10.1038/ni.3125
29. Paloschi V, Pauli J, Winski G, Wu Z, Li Z, Botti L, Meucci S, Conti P, Rogowitz F, Glukha N, et al. Utilization of an artery-on-a-chip to unravel novel regulators and therapeutic targets in vascular diseases. *Adv Healthc Mater*. 2024;13:1–19. doi: 10.1002/adhm.202302907
30. Fasolo F, Jin H, Winski G, Chernogubova E, Pauli J, Winter H, Li DY, Glukha N, Bauer S, Metschl S, et al. Long noncoding RNA MIAT controls advanced atherosclerotic lesion formation and plaque destabilization. *Circulation*. 2021;144:1567–1583. doi: 10.1161/CIRCULATIONAHA.120.052023
31. Alsaigh T, Evans D, Frankel D, Torkamani A. Decoding the transcriptome of calcified atherosclerotic plaque at single-cell resolution. *Commun Biol*. 2022;5:1–17.
32. Bashore AC, Yan H, Xue C, Zhu LY, Kim E, Mawson T, Coronel J, Chung A, Sachs N, Ho S, et al. High-dimensional single-cell multimodal landscape of human carotid atherosclerosis. *Arterioscler Thromb Vasc Biol*. 2024;44:930–945. doi: 10.1161/ATVBAHA.123.320524
33. Shen X, Liu Y, Hsu YJ, Fujiwara Y, Kim J, Mao X, Yuan GC, Orkin SH. EZH1 mediates methylation on histone H3 lysine 27 and Complements EZH2 in maintaining stem cell identity and executing pluripotency. *Mol Cell*. 2008;32:491–502. doi: 10.1016/j.molcel.2008.10.016
34. Sawada S, Scarborough JD, Killeen N, Littman DR. A lineage-specific transcriptional silencer regulates CD4 gene expression during T lymphocyte development. *Cell*. 1994;77:917–929. doi: 10.1016/0092-8674(94)90140-6
35. Maekawa Y, Minato Y, Ishifune C, Kurihara T, Kitamura A, Kojima H, Yagita H, Sakata-Yanagimoto M, Saito T, Taniuchi I, et al. Notch2 integrates signaling by the transcription factors RBP-J and CREB1 to promote T cell cytotoxicity. *Nat Immunol*. 2008;9:1140–1147. doi: 10.1038/ni.1649
36. Virmani R, Kolodgie FD, Burke AP, Farb A, Schwartz SM. Lessons From Sudden Coronary Death. *Arterioscler Thromb Vasc Biol*. 2000;20:1262–1275. doi: 10.1161/01.atv.20.5.1262
37. Veillard NR, Steffens S, Pelli G, Lu B, Kwak BR, Gerard C, Charo IF, Mach F. Differential influence of chemokine receptors CCR2 and CXCR3 in development of atherosclerosis in vivo. *Circulation*. 2005;112:870–878. doi: 10.1161/CIRCULATIONAHA.104.520718
38. Lacy M, Bürger C, Shami A, Ahmadsei M, Winkels H, Nitz K, van Tiel CM, Seijkens TTP, Kusters RJJ, Karshovka E, et al. Cell-specific and divergent roles of the CD40L-CD40 axis in atherosclerotic vascular disease. *Nat Commun*. 2021;12:1–12.
39. Nitz K, Lacy M, Bianchini M, Wichapong K, Kücüköge IA, Bonfiglio CA, Migheli R, Wu Y, Bürger C, Li Y, et al. The amino acid homoarginine inhibits atherogenesis by modulating t-cell function. *Circ Res*. 2022;131:701–712. doi: 10.1161/CIRCRESAHA.122.321094
40. Yamamoto J, Adachi Y, Onoue Y, Adachi YS, Okabe Y, Itazawa T, Toyoda M, Seki T, Morohashi M, Matsushima K, et al. Differential expression of the chemokine receptors by the Th1- and Th2-type effect or populations within circulating CD4+ T cells. *J Leukoc Biol*. 2002;68:568–574. doi: 10.1189/jlb.68.4.568
41. Janjic A, Wange LE, Bagnoli JW, Geuder J, Nguyen P, Richter D, Vieth B, Vick B, Jeremias I, Ziegenhain C, et al. Prime-seq, efficient and powerful bulk RNA-sequencing. *Genome Biol*. 2022;23:88. doi: 10.1186/s13059-022-02660-8
42. Harsha K, Krovi S, Zhang J, Michaels-Foster MJ, Brunetti T, Loh L, Scott-Brownie J, Gapin L. Thymic iNKT single cell analyses unmask the common developmental program of mouse innate T cells. *Nat Commun*. 2020;11:6238. doi: 10.1038/s41467-020-20073-8
43. Baranek T, Lebrigand K, de Amat Herbozo C, Gonzalez L, Bogard G, Dietrich C, Magnone V, Boisseau C, Jouan Y, Trottein F, et al. High dimensional single-cell analysis reveals iNKT cell developmental trajectories and effector fate decision. *Cell Rep*. 2020;32:108116. doi: 10.1016/j.celrep.2020.108116
44. Vivier E, Ugolini S, Blaise D, Chabannon C, Brossay L. Targeting natural killer cells and natural killer T cells in cancer. *Nat Rev Immunol*. 2012;12:239–252. doi: 10.1038/nri3174
45. Das R, Sant'Angelo DB, Nichols KE. Transcriptional control of invariant NKT cell development. *Immunity Rev*. 2010;238:195–215. doi: 10.1111/j.1600-065X.2010.00962.x
46. Salio M, Silk JD, Yvonne Jones E, Cerundolo V. Biology of CD1- and MR1-restricted T cells. *Annu Rev Immunol*. 2014;32:323–366. doi: 10.1146/annurev-immunol-032713-120243
47. Lee YJ, Holzapfel KL, Zhu J, Jameson SC, Hogquist KA. Steady-state production of IL-4 modulates immunity in mouse strains and is determined by lineage diversity of iNKT cells. *Nat Immunol*. 2013;14:1146–1154. doi: 10.1038/ni.2731
48. Krovi SH, Gapin L. Invariant natural killer T cell subsets—more than just developmental intermediates. *Front Immunol*. 2018;9:1–17.
49. Su IH, Dobenecker MW, Dickinson E, Oser M, Basavaraj A, Marqueron R, Viale A, Reinberg D, Wülfing C, Tarakhovskiy A. Polycomb group protein Ezh2 controls actin polymerization and cell signaling. *Cell*. 2005;121:425–436. doi: 10.1016/j.cell.2005.02.029
50. Buono C, Binder CJ, Stavrakis G, Witztum JL, Glimcher LH, Lichtman AH. T-bet deficiency reduces atherosclerosis and alters plaque antigen-specific immune responses. *Proc Natl Acad Sci U S A*. 2005;102:1596–1601. doi: 10.1073/pnas.0409015102
51. Buono C, Come CE, Stavrakis G, Maguire GF, Connelly PW, Lichtman AH. Influence of interferon- $\gamma$  on the extent and phenotype of diet-induced atherosclerosis in the LDLR-deficient mouse. *Arterioscler Thromb Vasc Biol*. 2003;23:454–460. doi: 10.1161/01.ATV.0000059419.11002.6E
52. Gupta S, Pablo AM, Jiang XC, Wang N, Tall AR, Schindler C. IFN- $\gamma$  potentiates atherosclerosis in ApoE knock-out mice. *J Clin Invest*. 1997;99:2752–2761. doi: 10.1172/JCI119465
53. King VL, Cassis LA, Daugherty A. Interleukin-4 does not influence development of hypercholesterolemia or angiotensin II-induced atherosclerotic lesions in mice. *Am J Pathol*. 2007;171:2040–2047. doi: 10.2353/ajpath.2007.060857
54. King VL, Szilvassy SJ, Daugherty A. Interleukin-4 deficiency decreases atherosclerotic lesion formation in a site-specific manner in female LDL receptor-/- mice. *Arterioscler Thromb Vasc Biol*. 2002;22:456–461. doi: 10.1161/hq0302.104905
55. Cardillo-Reis L, Gruber S, Schreiber SM, Drechsler M, Papac-Milicevic N, Weber C, Wagner O, Stangl H, Soehnlein O, Binder CJ. Interleukin-13 protects from atherosclerosis and modulates plaque composition by skewing the macrophage phenotype. *EMBO Mol Med*. 2012;4:1072–1086. doi: 10.1002/emmm.201201374
56. Junttila IS. Tuning the cytokine responses: An update on interleukin (IL)-4 and IL-13 receptor complexes. *Front Immunol*. 2018;9:888. doi: 10.3389/fimmu.2018.00888
57. Rahman K, Vengrenyuk Y, Ramsey SA, Vila NR, Girgis NM, Liu J, Gusarova V, Gromada J, Weinstock A, Moore KJ, et al. Inflammatory Ly6Chi monocytes and their conversion to M2 macrophages drive atherosclerosis regression. *J Clin Invest*. 2017;127:2904–2915. doi: 10.1172/JCI75005
58. Weinstock A, Rahman K, Yaacov O, Nishi H, Menon P, Ninkain CA, Garabedian ML, Pena S, Akbar N, Sansbury BE, et al. Wnt signaling enhances macrophage responses to IL-4 and promotes resolution of atherosclerosis. *Elife*. 2021;10:1–28.
59. Godfrey DI, Uldrich AP, McCluskey J, Rossjohn J, Moody DB. The burgeoning family of unconventional T cells. *Nat Immunol*. 2015;16:1114–1123. doi: 10.1038/ni.3298
60. Klibi J, Amable L, Benlagha K. A focus on natural killer T-cell subset characterization and developmental stages. *Immunity Cell Biol*. 2020;98:358–368. doi: 10.1111/imcb.12322

61. Nakai Y, Iwabuchi K, Fujii S, Ishimori N, Dashtsoodol N, Watano K, Mishima T, Iwabuchi C, Tanaka S, Bezbradica JS, et al. Natural killer T cells accelerate atherogenesis in mice. *Blood*. 2004;104:2051–2059. doi: 10.1182/blood-2003-10-3485
62. Li Y, Kanellakis P, Hosseini H, Cao A, Deswaerte V, Tipping P, Toh BH, Bobik A, Kyaw T. A CD1d-dependent lipid antagonist to NKT cells ameliorates atherosclerosis in ApoE<sup>-/-</sup> mice by reducing lesion necrosis and inflammation. *Cardiovasc Res*. 2016;109:305–317. doi: 10.1093/cvr/cvv259
63. Semmling V, Lukacs-Kornek V, Thaiss CA, Quast T, Hochheiser K, Panzer U, Rossjohn J, Perlmutter P, Cao J, Godfrey DI, et al. Alternative cross-priming through CCL17-CCR4-mediated attraction of CTLs toward NKT cell-licensed DCs. *Nat Immunol*. 2010;11:313–320. doi: 10.1038/ni.1848
64. Kragten NA, Taggenbrock RL, Parga Vidal L, van Lier RA, Stark R, van Gisbergen KP, Hobit and Blimp-1 instruct the differentiation of iNKT cells into resident-phenotype lymphocytes after lineage commitment. *Eur J Immunol*. 2022;52:389–403. doi: 10.1002/eji.202149360
65. Slauenwhite D, Johnston B. Regulation of NKT cell localization in homeostasis and infection. *Front Immunol*. 2015;6:255. doi: 10.3389/fimmu.2015.00255
66. Arvey A, Van Der Veecken J, Samstein RM, Feng Y, Stamatoyannopoulos JA, Rudensky AY. Inflammation-induced repression of chromatin bound by the transcription factor Foxp3 in regulatory T cells. *Nat Immunol*. 2014;15:580–587. doi: 10.1038/ni.2868
67. Yang XP, Jiang K, Hirahara K, Vahedi G, Afzali B, Sciume G, Bonelli M, Sun HW, Jankovic D, Kanno Y, et al. EZH2 is crucial for both differentiation of regulatory T cells and T effector cell expansion. *Sci Rep*. 2015;5:1–14. doi: 10.1038/srep10643
68. Ait-Oufella H, Salomon BL, Potteaux S, Robertson AKL, Gourdy P, Zoll J, Merval R, Esposito B, Cohen JL, Fisson S, et al. Natural regulatory T cells control the development of atherosclerosis in mice. *Nat Med*. 2006;12:178–180. doi: 10.1038/nm1343
69. Wolf D, Gerhardt T, Winkels H, Michel NA, Pramod AB, Ghosheh Y, Brunel S, Buscher K, Miller J, McArdle S, et al. Pathogenic autoimmunity in atherosclerosis evolves from initially protective apolipoprotein B100-reactive CD4+T-regulatory cells. *Circulation*. 2020;142:1279–1293. doi: 10.1161/CIRCULATIONAHA.119.042863
70. Wei X, Zhang Y, Xie L, Wang K, Wang X. Pharmacological inhibition of EZH2 by GSK126 decreases atherosclerosis by modulating foam cell formation and monocyte adhesion in apolipoprotein E-deficient mice. *Exp Ther Med*. 2021;22:841.10.3892/etm.2021.10273
71. Neele AE, Chen HJ, Gijbels MJJ, van der Velden S, Hoeksema MA, Boshuizen MCS, Van den Bossche J, Tool AT, Matlung HL, van den Berg TK, et al. Myeloid Ezh2 deficiency limits atherosclerosis development. *Front Immunol*. 2021;11:1–9.
72. Duan R, Du W, Guo W. EZH2: A novel target for cancer treatment. *J Hematol Oncol*. 2020;13:1–12.
73. Kang N, Eccleston M, Clermont PL, Latarani M, Male DK, Wang Y, Crea F. EZH2 inhibition: A promising strategy to prevent cancer immune editing. *Epigenomics*. 2020;12:1457–1476. doi: 10.2217/epi-2020-0186
74. Sary HC, Chandler A, Dinsmore RE, Fuster V, Glagov S, Insull JW, Rosenfeld ME, Schwartz CJ, Wagner WD, Wissler RW. A definition of advanced types of atherosclerotic lesions and a histological classification of atherosclerosis: a report from the Committee on Vascular Lesions of the Council on Arteriosclerosis, American Heart Association. *Circulation*. 1995;92:1355–1374. doi: 10.1161/01.cir.92.5.1355
75. Redgrave JN, Gallagher P, Lovett JK, Rothwell PM. Critical cap thickness and rupture in symptomatic carotid plaques: The oxford plaque study. *Stroke*. 2008;39:1722–1729. doi: 10.1161/STROKEAHA.107.507988
76. Gayoso A, Shor J. JonathanShor/DoubletDetection: doubletdetection v3.0. Zenodo. Accessed February 4, 2025. <https://zenodo.org/records/6349352>
77. Wolf FA, Philipp A, Theis FJ. SCANPY: large-scale single-cell gene expression data analysis. *Genome Biol*. 2018;19:15. doi: 10.1186/s13059-017-1382-0
78. Söderholm S, Jauregi-Miguel A, Pagella P, Ghezzi V, Zambanini G, Nordin A, Cantù C. Single-cell response to Wnt signaling activation reveals uncoupling of Wnt target gene expression. *Exp Cell Res*. 2023;429:113646. doi: 10.1016/j.yexcr.2023.113646
79. Santovito D, Henderson J, Bidzhekov K, Triantafyllidou V, Jansen Y, Chen Z, Farina F, Diagal A, Aslani M, Blanchet X, et al. Mex3a protects against atherosclerosis: evidence from mice and humans. *Circulation*. 2024;150:1213–1216. doi: 10.1161/CIRCULATIONAHA.124.069526
80. Trapnell C, Cacchiarelli D, Grimsby J, Pokharel P, Li S, Morse M, Lennon NJ, Livak KJ, Mikkelsen TS, Rinn JL. The dynamics and regulators of cell fate decisions are revealed by pseudotemporal ordering of single cells. *Nat Biotechnol*. 2014;32:381–386. doi: 10.1038/nbt.2859
81. Hao Y, Hao S, Andersen-Nissen E, Mauck WM, Zheng S, Butler A, Lee MJ, Wilk AJ, Darby C, Zager M, et al. Integrated analysis of multimodal single-cell data. *Cell*. 2021;184:3573–3587.e29. doi: 10.1016/j.cell.2021.04.048
82. Mohanta SK, Peng L, Li Y, Lu S, Sun T, Carnevale L, Perrotta M, Ma Z, Förster B, Stanic K, et al. Neuroimmune cardiovascular interfaces control atherosclerosis. *Nature*. 2022;605:152–159. doi: 10.1038/s41586-022-04673-6
83. Fedoseienko A, Wijers M, Wolters JC, Dekker D, Smit M, Huijckman N, Kloosterhuis N, Klug H, Schepers A, Van Dijk KW, et al. The COMMD family regulates plasma LDL levels and attenuates atherosclerosis through stabilizing the CCC complex in endosomal LDLR trafficking. *Circ Res*. 2018;122:1648–1660. doi: 10.1161/CIRCRESAHA.117.312004
84. Renaud G, Stenzel U, Maricic T, Wiebe V, Kelso J, DeML. Robust demultiplexing of Illumina sequences using a likelihood-based approach. *Bioinformatics*. 2015;31:770–772. doi: 10.1093/bioinformatics/btu719
85. Fleming SJ, Chaffin MD, Arduini A, Akkad AD, Banks E, Marioni JC, Philippakis AA, Ellinor PT, Babadi M. Unsupervised removal of systematic background noise from droplet-based single-cell experiments using CellBender. *Nat Methods*. 2023;20:1323–1335. doi: 10.1038/s41592-023-01943-7
86. Miller SA, Policastro RA, Sriramkumar S, Lai T, Huntington TD, Ladaika CA, Kim D, Hao C, Zentner GE, O'Hagan HM. LSD1 and aberrant DNA methylation mediate persistence of enteroendocrine progenitors that support BRAF-mutant colorectal cancer. *Cancer Res*. 2021;81:3791–3805. doi: 10.1158/0008-5472.CAN-20-3562
87. Parekh S, Ziegenhain C, Vieth B, Enard W, Hellmann I. zUMIs - A fast and flexible pipeline to process RNA sequencing data with UMIs. *GigaScience*. 2018;7:1–9.
88. Dobin A, Davis CA, Schlesinger F, Drenkow J, Zaleski C, Jha S, Batut P, Chaisson M, Gingeras TR. STAR: ultrafast universal RNA-seq aligner. *Bioinformatics*. 2013;29:15–21. doi: 10.1093/bioinformatics/bts635
89. Robinson MD, McCarthy DJ, Smyth GK. edgeR: A Bioconductor package for differential expression analysis of digital gene expression data. *Bioinformatics*. 2009;26:139–140. doi: 10.1093/bioinformatics/btp616
90. Kuleshov MV, Jones MR, Rouillard AD, Fernandez NF, Duan Q, Wang Z, Koplev S, Jenkins SL, Jagodnik KM, Lachmann A, et al. Enrichr: a comprehensive gene set enrichment analysis web server 2016 update. *Nucleic Acids Res*. 2016;44:W90–W97. doi: 10.1093/nar/gkw377
91. Xie Z, Bailey A, Kuleshov MV, Clarke DJB, Evangelista JE, Jenkins SL, Lachmann A, Wojciechowicz ML, Kropiwnicki E, Jagodnik KM, et al. Gene set knowledge discovery with Enrichr. *Curr Protoc*. 2021;1:e90. doi: 10.1002/cpz1.90
92. Zhou Y, Zhou B, Pache L, Chang M, Khodabakhshi AH, Tanaseichuk O, Benner C, Chanda SK. Metascape provides a biologist-oriented resource for the analysis of systems-level datasets. *Nat Commun*. 2019;10:1523. doi: 10.1038/s41467-019-09234-6
93. Waskom M. Seaborn: statistical data visualization. *J Open Source Softw*. 2021;6:3021. doi: 10.21105/joss.03021
94. Hammelman J, Patel T, Closser M, Wichterle H, Gifford D. Ranking reprogramming factors for cell differentiation. *Nat Methods*. 2022;19:812–822. doi: 10.1038/s41592-022-01522-2
95. Cohen NR, Brennan PJ, Shay T, Watts GF, Brigl M, Kang J, Brenner MB, Monach P, Shinton SA, Hardy RR, et al. Shared and distinct transcriptional programs underlie the hybrid nature of iNKT cells. *Nat Immunol*. 2013;14:90–99. doi: 10.1038/ni.2490
96. Robinson JT, Thorvaldsdóttir H, Winckler W, Guttman M, Lander ES, Getz G, Mesirov JP. Integrative genomics viewer. *Nat Biotechnol*. 2011;29:24–26. doi: 10.1038/nbt.1754